INVESTIGATION OF THE FUNCTION AND REGULATION OF THE TRPM7 ION CHANNEL IN THE RENAL PROXIMAL TUBULE

by

LIPING LOU

A dissertation submitted to the

School of Graduate Studies

Rutgers, The State University of New Jersey

In partial fulfillment of the requirements

For the degree of

Doctor of Philosophy

Graduate Program in Cellular and Molecular Pharmacology

Written under the direction of

Loren W. Runnels, Ph.D.

And approved by

_____

_____

_____

_____

_____

New Brunswick, New Jersey

May, 2019

ABSTRACT OF THE DISSERTATION

INVESTIGATION OF THE FUNCTION AND REGULATION OF THE TRPM7 ION CHANNEL IN THE RENAL PROXIMAL TUBULE

By LIPING LOU

Dissertation Director:

Loren W. Runnels, Ph.D.

The TRPM7 (Transient Receptor Potential Melastatin 7) ion channel is a unique member of the TRP channel family, possessing its own functional kinase domain at its COOH-terminus. As a Mg^{2+}-permeable ion channel, TRPM7 has frequently been linked to the regulation of magnesium reabsorption at both the cellular and whole-body level. Mg^{2+} plays a pivotal role in human health and disease, and therefore, its level in the body has to be tightly regulated via ion channels and transporters in the functional unit of the kidney, the nephron. TRPM6, the close homolog of TRPM7, has been identified to be the major player regulating Mg^{2+} reabsorption in the distal convoluted tubule of the nephron. A major gap in our knowledge of TRPM7 is whether the channel is involved in regulating magnesium homeostasis in the proximal tubule of the nephron, where TRPM7 is highly expressed.

To gain insight into the function of TRPM7 in the proximal tubule, we generated two conditional strains of proximal tubule-specific *trpm7 KO* mice, using PEPCK-Cre and

gGT-Cre mice. The Mg^{2+} status of the proximal tubule *trpm7* knockout mice was assessed but we did not obtain any evidence that the Mg^{2+} homeostasis was disrupted in the animals, indicating TRPM7 does not play a major role in proximal tubule to regulate whole-body magnesium homeostasis. However, large cavities and reduced cortical layers in the kidney anatomy of some female gGT-Cre *KO trpm7* mice were observed. TRPM7 has previously been implicated in the regulation of cell-cell adhesion, having recently been found to contribute to the intercellular junction formation in the bladder urothelium. We performed transmission electron microscopy (TEM) analysis of the tissue slides obtained from the cortex of the kidneys from gGT-Cre *KO trpm7* mice and found that tubule epithelial cells from the *trpm7 KO* mice had more impaired intercellular junctions than that from the control mice.

We next investigated the relationship between TRPM7 and cell-cell adhesion process, employing the proximal tubule epithelial cell line, opossum kidney (OK) cells, as a cellular model. Mass spectrometric analysis uncovered that TRPM7 interacted with a cell adhesion protein called plakoglobin. Using immunocytochemical assays, we discovered that TRPM7 co-localized with plakoglobin and another adherens junction protein called E-cadherin. Application of the TRPM7's channel blocker NS8593 to OK cells reduced E-cadherin expression and localization to adherens junctions. Taken together, these data suggest that TRPM7 is involved in controlling cell-cell adhesion in proximal tubule epithelial cells.

In this study, we also explored the mechanism(s) by which TRPM7's cellular localization is regulated. Using biochemical and immunocytochemical approaches, we identified a regulatory site at the COOH-terminus of TRPM7, the channel's PDZ-binding motif, through which the localization of TRPM7 in OK cells could be regulated. Deletion

of the channel's PDZ-binding motif shortened the retention time of the mutant TRPM7 (TRPM7ΔPDZ) at adherens junctions of OK cells. We also discovered that TRPM7's localization to the adherens junctions in OK cells was potentiated by the activation of PKC, indicating that TRPM7 localization is potentially regulated by the PKC pathway.

While our understanding of the relationship between TRPM7 and cell-cell adhesion is still in its infancy, the discoveries made in this study will guide future investigations into the physiological roles of the channel in the regulation of cell-cell adhesion.

ACKNOWLEDGMENTS

First and foremost, I want to thank my advisor, Dr. Loren W. Runnels for his great mentorship, both in science and in life. Loren is a great scientist and educator with enormous enthusiasm and devotion to research. Under his guidance, I have learned how to ask important questions, conduct scientific research, and present my research work. Initially, I joined his lab with zero biology knowledge and background. Still, he was able to train me to be a qualified cell biologist. I deeply appreciate his guidance and support throughout all these years of my Ph.D. study. Yet, what I admire the most about him is the big heart he has and the work he is doing to make this world a better place. The time I spent in Loren's lab will be a great asset for me in my future life and career.

For this dissertation, I would like to express my sincere gratitude to my thesis committee members, Dr. Huizhou Fan, Dr. Alexey G. Ryazanov, and Dr. Federico Sesti, for their time, interest, and helpful discussion. Their insightful feedback and advice during every committee meeting were invaluable for the progress of my project.

The members of the Runnels lab have contributed immensely to my personal and professional time at Rutgers. The first one I want to thank is my twin sister in the lab, Na Cai, who is now pursuing her dreams at Merck, California. She, as someone used to refer to me, is a "tough cookie"- sweet and strong. I admire her so much that she is always so competent and confident, and attentive to people who ask for her help. I am so thankful for her help and support during my Ph.D. study. I would also like to thank the current members in our lab, Namariq Al-Saadi and Sandra Tetteh, for their support and company. I will never forget the surprising birthday parties that you guys had thrown for me. I am so glad that I had the opportunity to work with such caring and hearty people like you. I also want to thank the former members of the Runnels lab: Yuko Komiya, for sharing many of her

research techniques with me, and Zhiyong Bai., Jeffrey Overton, Omayra Gonzalez-Pagan, and Shufei Tao for the help I have received from them. My sincere thanks also go to the faculty, students and staff members of the Molecular Bioscience Program and the Pharmacology department for being such a great source of friendship as well as good advice and collaboration.

I gratefully acknowledge the funding sources that have supported my Ph.D. work. During my Ph.D. study, I have been funded by the fellowships from Rutgers Graduate School of Biomedical Sciences, and the American Heart Association Predoctoral fellowship. My work was also supported by the National Institute of Health and New Jersey Commission on Brain Injury Research.

My time at Rutgers was made enjoyable and unforgettable in large part due to the many friends that became a part of my life. I want to thank my best friends, Wenchun Xie and Na Cai, who have always been there for me and supported me during difficult times. I am also grateful for the company and supports of many friends: Tianle Yang, Qichen Wang, Chen Wang, Jin Ling, Wurihan, Huirong Zhang, Zhichao Song, Hamidah Raduwan, Sai Zhang, Bola Olayanju, Edgar Ferrer González, Yijun Zhou, Yuanwang Pan, Chengshen Zhu, Zhenru Zhou, Jie wang, and many more.

Lastly, I would like to thank my family for all their unconditional love and encouragement. For my parents who raise me with love and supported me in all my pursuits. For my beloved sister, who has been sending my 14-month-old nephew's videos to me to help reduce my stress level during my thesis writing process. For my mother-in-law, Gregoria Gamarra, who always supports me and is proud of me. And most of all for my loving, encouraging, supportive, and patient best friend in life, my husband Zak-id

Gamarra, whose faithful support during every stage of this Ph.D. is so appreciated. Thank you and may God bless you!

Liping Lou

Rutgers University

April 2019

TABLE OF CONTENTS

LIST OF FIGURES

INTRODUCTION

Transient receptor potential (TRP) channels play essential roles in sensing environmental stimuli and conducting those signals into cells. Mammalian TRP channels respond to a wide range of stimuli including light, cold, heat, sweet, bitter, and pain, as well as neurotransmitters, hormones, and growth factors [1]. There are six mammalian TRP channel subfamilies. TRPM7 belongs to the subfamily M (Melastatin). Soon after its identification, TRPM7 has emerged as a ubiquitously expressed protein with many potential physiological roles ascribed to it, including regulation of cellular and whole body Mg^{2+} homeostasis, embryonic development, cell proliferation, cell adhesion, and cell stress [2]. Despite many important roles that TRPM7 plays at both the cellular and whole-body level, our understanding of the functions and regulations of TRPM7 are still very limited. The purpose of this dissertation is to investigate the function of TRPM7 in renal proximal tubule, where the channel has high level of expression, but where the function of the TRPM7 remains unknown. In this introduction, I will give an overview of the essential background on TRPM7's channel properties and its functions, which will give the context for understanding the rationale of this study.

1. TRPM7

TRPM7 (Transient Receptor Potential Melastatin), also known as TRP-PLIK, ChaK1, and LTRPC7, is a transient receptor potential ion channel coupled to an alpha-type Ser/Thr kinase domain[2-4]. The human TRPM7 gene locates on chromosome 15, contains 39 exons encoding 1863 amino acids. The TRPM7 channel is formed as a multimeric complex, which is considered to be composed of four subunits that contribute to form the channel pore. Each channel subunit has a melastatin segment on its N-terminus followed

by six transmembrane helices harboring a pore-forming loop between helices 5 and 6. On its COOH-terminus, TRPM7 successively contains a highly conserved transient receptor potential (TRP) domain, a coiled-coil domain, a kinase substrate Serine/Threonine domain, and finally an alpha-kinase domain (Figure 1A). At TRPM7's extreme COOH-terminus, TRPM7 contains putative PDZ-binding motif, which may allow it to bind to PDZ-containing proteins, as we will discuss below. Among all ion channels, TRPM7 and its homologous protein, TRPM6 (also known as TRP-PLIK2, ChaK2, and LTRPC6) are the only two members that possess their own kinase domains [2].

TRPM7 is a ubiquitously expressed protein and native TRPM7 currents have been detected in all cell types investigated so far [2-5]. The TRPM7 current constitutes a strong outwardly rectifying conductance carried by K^+ at positive potentials and a small inward conductance carried exclusively by divalent cations such as Mg^{2+}, and Ca^{2+} and Zn^{2+} at negative potentials (Figure 1B) [4]. TRPM7 is also highly permeable to other essential divalent cations, including Zn^{2+}, Mn^{2+}, Co^{2+}, and the non-physiological or even toxic cations Ba^{2+}, Sr^{2+}, Ni^{2+}, and Cd^{2+}, suggesting that TRPM7 may be responsible for the influx of the trace metals into cells [6]. TRPM7 is considered to be a constitutively active channel and is negatively regulated by intracellular divalent cations (Mg^{2+}, Ba^{2+}, Sr^{2+}, Zn^{2+}, Mn^{2+}), Mg·ATP, chloride (Cl^-) and bromide (Br^-), polyamines, reduction of intracellular pH and hydrolysis of the acidic phospholipid phosphatidylinositol 4,5-bisphosphate (PIP_2) [6-10].

The kinase domain of TRPM7 belongs to a family of protein kinases called alpha-kinases, which has no detectable sequence homology to conventional protein kinases. Unlike the conventional protein kinases, whose phosphorylation sites locate within loops, turns or irregular structures, the alpha-kinase family phosphorylate amino acids located in the coiled-coil alpha-helical region of its substrates [11, 12]. TRPM7 autophosphorylates

and the substrates for TRPM7 kinase that have been identified so far, include annexin A1, myosin IIA's heavy chain and PLCγ2 [13-16]. It was found that TRPM7 kinase also played a role in regulating the phosphorylation of eukaryotic elongation factor 2 (eEF2) via the activation of eEF2-kinase [17].

The kinase activity of TRPM7 was reported to be controlled through the autophosphorylation of a serine/threonine rich region located *N*-terminal to the catalytic domain [18-20]. Using Mass spectrometric analysis, Cai et al recently identified two phosphorylation sites, S1565, in TRPM7's exchange domain, and S1777, in TRPM7's catalytic domain, as potential regulatory sites of TRPM7's kinase activity [21]. They discovered that the phosphorylation of these two sites inactivate TRPM7's kinase activity, with phosphorylation of S1777 functioning as a stop signal for TRPM7 catalysis, and phosphorylation of S1565 functioning as a regulatory switch to control TRPM7 catalytic activity.

The role of the kinase domain in controlling TRPM7 channel function remains incompletely understood [15]. Results from several labs revealed that it was the kinase domain itself rather than its catalytic activity that is crucial for channel function [4, 7, 8, 22-24]. Deletion of the whole kinase domain led to an apparently inactive channel, while the mutations that abolished the kinase's catalytic activity did not alter the channel activity, as measured by whole-cell recording or Ca^{2+} influx, indicating that the kinase domain may play a structural role in channel assembly or subcellular localization [23, 24]. A recent study published Cai and colleagues revealed that the kinase activity affects turnover of the protein and channel localization in polarized epithelial cells [25].

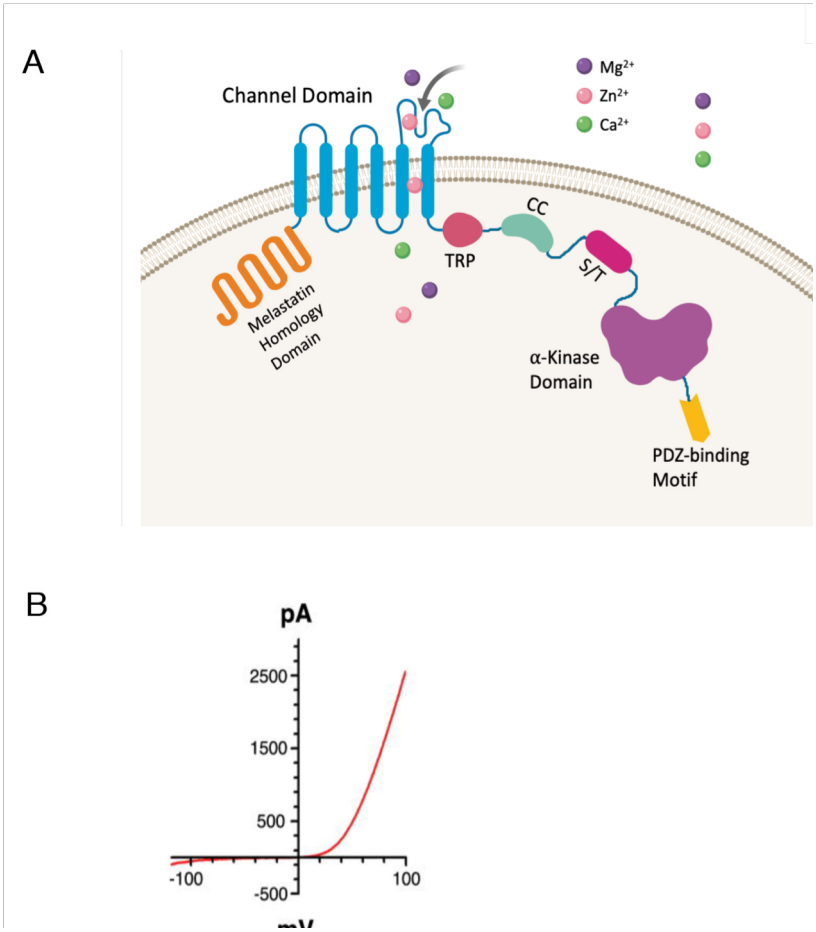

Figure 1. The structure and channel properties of the TRPM7 ion channel

(A). From left to right, the TRPM7 ion channel-kinase contains a melastatin domain that is homologous to other members in TRPM subfamily, a six-transmembrane domain, which forms the channel pore by the loop between the fifth and six transmembrane domain, followed by a short TRP domain which is essential for the regulation of channel gating, a coiled coil domain, a Serine/Threonine rich domain followed by an alpha-kinase domain, and finally a short peptide sequence called PDZ-binding motif on the C-terminus,. TRPM7 is permeable to a series of divalent cations, such as Mg^{2+}, Zn^{2+} and Ca^{2+}. **(B).** Whole-cell

current of TRPM7 measured by patch clamp electrophysiology. TRPM7 current shows a strong outwardly rectifying conductance at positive potentials carried by K^+, and a small inward conductance at negative potentials carried by divalent cations such as Mg^{2+}, Ca^{2+} and Zn^{2+}.

2. The function of TRPM7

TRPM7 play an essential role in many physiological and pathological processes. As a Mg^{2+}-, Ca^{2+}- and Zn^{2+}- permeable ion channel, TRPM7 modulates intracellular Mg^{2+}, Ca^{2+} and Zn^{2+} levels [4, 9, 14, 22, 26-28]. It is also an important regulator of cell survival, cell proliferation, cell differentiation, and cell motility [4, 14, 22, 24, 29-39]. TRPM7 has been reported to be involved in the process of immune system [33, 40], exocytosis [41], mechanosensitivity [42], and regulation of cytoskeletal architecture [15]. Dysfunction of TRPM7 in human body is associated with cardiac fibrosis [43], hypertension [44, 45], neurodegenerative disease, anoxic neuronal death [46], and tumor growth and metastasis [47, 48] .

Global deletion of TRPM7 in mouse caused embryonic lethality, before embryonic day 7.5 (E7.5) [49]. In contrast, time restricted deletion of TRPM7 using tamoxifen-inducible *Cre-ER* transgenic line performed at E14.5 or in adult mice did not result in any morphological or obvious behavioral abnormalities [50]. These results suggested that TRPM7 had a nonredundant and vital role in early embryogenesis. Studies in zebrafish showed that disruption of *Trpm7* caused kidney stone formation, defects in skeletogenesis and albinism [51]. In *Xenopus laevis* frogs, depletion of TRPM7 using antisense morpholino oligonucleotides led to severe gastrulation defects, which could be rescued by Mg^{2+} supplementation [52].

Tissue-specific deletion of TRPM7 in the T cell lineage from mouse disrupted thymopoiesis, the process of differentiation of thymocytes into mature T cells. The disruption led to dysregulation of synthesis of many growth factors that are essential for the differentiation and maintenance of thymic epithelial cells, which resulted in developmental block of thymocytes and a depletion of thymic medullary cells [49]. In the kidney, TRPM7 was found essential for kidney development from metanephric mesenchyme (MM), but not the ureteric bud, indicating a spatiotemporal requirement for TRPM7 during kidney development[50]. Targeted disruption of TRPM7 in the metanephric mesenchyme caused a reduction in glomeruli number, generation renal cysts in proximal tubule and renal tubular dilation [50]. Studies in urothelium-specific *Trpm7 KO* mice revealed that TRPM7 is involved in the formation of intercellular adhesion junctions in mouse urothelium [53].

3. TRPM7 and magnesium homeostasis

TRPM7 and TRPM6 garnered much interest upon their discovery as the first ion channels to possess their own kinase domains. Soon after their identification, the two proteins were quickly linked to the regulation of magnesium reabsorption at both the cellular and whole-body level [5, 22, 26, 54-57]. Schmitz et al reported that targeted deletion of TRPM7 in cells caused cell growth arrest within 24 h and eventually cell death. However, the above phenotype could be rescued by supplementation of the growth media with 10 mM Mg^{2+}[22]. Likewise, some of the phenotypes resulting from loss of *Trpm7* in zebrafish and *Xenopus leavis* could also be rescued by magnesium supplementation [51, 52]. In 2002, two separate groups identified TRPM6 as the gene responsible for a rare autosomal disorder called familial hypomagnesemia with secondary hypocalcemia (HSH), which is

characterized by very low magnesium and low calcium serum levels [58, 59]. Affected individuals exhibit neurologic symptoms of hypomagnesemic hypocalcemia, including seizures and muscle spasm, shortly after birth, which can be corrected by oral magnesium supplementation.

While a majority of the mutations in individuals affected with HSH are either nonsense or frameshift mutations easily compatible with a loss-of-function phenotype, one missense mutation entails the exchange of a highly conserved serine for a leucine at amino acid position 141. Surprisingly, Chubanov and colleagues showed that the S141L mutation disables the ability of TRPM6 to form multimers with TRPM7 for efficient trafficking to the plasma membrane, which was the first evidence pointing a role for TRPM7 in whole-body magnesium [54]. Studies in mice have since confirmed a role for TRPM7 in Mg^{2+} homeostasis. Ryazanova et al investigated the TRPM7-deficient mice with deletion of the kinase domain of TRPM7. They found that the homozygous mutagenic mice demonstrated early embryonic lethality, whereas the heterozygous mice were viable but developed hypomagnesaemia caused by the defect in intestinal absorption [26]. The same group also generated and studied the mutagenic mice carrying inactive TRPM7 kinase and they discovered that these mice were resistant to dietary Mg^{2+} deprivation and survived three times longer than wild-type mice. They concluded that TRPM7 kinase acted as a sensor of Mg^{2+} status and that the kinase is involved in the coordination of cellular and systemic responses to Mg^{2+} deprivation [55]. Mittermeier et al recently reported that TRPM7 is the central gatekeeper of mineral intestinal absorption, which is essential for postnatal survival, indicating a critical role for TRPM7 in Mg^{2+} homeostasis [60].

4. NHERF proteins and TRPM7's regulation

TRPM7 has an important role in controlling the Mg^{2+} homeostasis in human body. Understanding the regulation mechanisms involved in controlling TRPM7 will help to establish more rational therapeutic approaches for treating disorders of mineral metabolism and chronic kidney diseases. To identify potential regulators for TRPM7 in kidney, we performed a yeast-two-hybrid screen against a mouse kidney library using the COOH-terminus of TRPM7 (a.a.1288-1863) and identified NHERF3 and NHERF4 as potential interacting proteins. NHERF3 and NHERF4 belong to a PDZ-scaffold protein family called NHERF, which stands for Na^+/H^+ Exchanger Regulatory Factor. Below we summarize what is known of the function and regulation of the four members in this family, NHERF1 (EBP50), NHERF2, NHERF3 (PDZK1) and NHERF4 (PDZK2).

The first member of the NHERF family, NHERF1 (EBP50) was first identified from the study of inhibition of Na^+/H^+ exchange transport by cAMP-dependent protein kinase A (PKA) in the brush-border membrane of the proximal tubule of the kidney[61]. NHERF1 was found to be responsible for facilitating the formation of a signal complex in PKA regulation of NHE3 (a Na^+/H^+ exchange transporter in proximal tubule). NHERF1 contains two PDZ domains (acronym of the postsynaptic density protein PSD-95, the *Drosophila* junctional protein Disc-large, and the tight junction protein ZO1). Additional members of the NHERF family were later identified and include NHERF2 (E3KARP), NHERF3 (PDZK1) and NHERF4 (IKEPP). NHERF1 and NHERF2 are composed of two protein-interactive PDZ domains and a COOH-terminal ezrin-binding domain (ERM domain) that can interact with the related cytoskeletal proteins, Moesin, Ezrin, Radixin and Merlin. NHERF3 and NHERF4 possess 4 PDZ domains but lack the carboxyl-terminal ezrin-binding domain found in NHERF1 and 2 (Figure 2). Since the PDZ domains can

form binding pockets for PDZ-binding motifs, a combination of 4-6 amino acids that are commonly, but not exclusively, found at the COOH terminus of ion channels and transporters, the NHERF proteins are usually involved in the formation of protein scaffolds by nucleating multiprotein complexes. The formation of multiprotein complexes is critical for many signal transduction pathways[62].

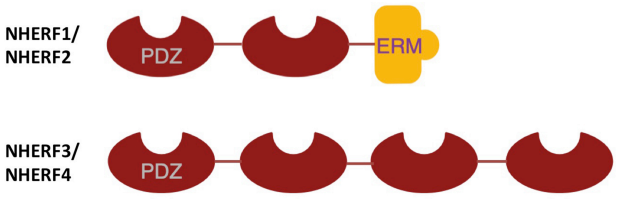

NHERF1 and NHERF2 are composed of two protein-interactive PDZ domains and a COOH-terminal ezrin-binding domain (ERM domain) that can interact with the related cytoskeletal proteins, Moesin, Ezrin, Radixin and Merlin (Top). NHERF3 and NHERF4 possess only 4 PDZ domains and lack the carboxyl-terminal ezrin-binding domain found in NHERF1 and 2 (Bottom).

PDZ domains are commonly used to mediate protein-protein interactions. PDZ domain containing proteins often have more than a single PDZ domain, which are employed to assemble and regulate multi-protein complexes. A classic example of this is the Drosophila INAD protein, a scaffolding protein with 5 PDZ domains that organizes the Rhodopsin regulated Drosophila TRP channel into a macromolecular complex with PLC (NorpA) and PKC (inaC) to control fly vision [63]. PDZ domain interactions with their ligands generally occur at the ligand COOH terminus and primarily involve amino acids at the last and third to last residue, although up to at least the last six amino acids can affect binding [64]. Generally, PDZ binding motifs can be subdivided into 3 classes: class I domains, which recognize the motif S/T-X-φ; class II domains, which recognize the motif φ-X-φ; and class III domains, which recognize the motif D/E-X-φ as their preferred C-terminal motif, where φ represents a hydrophobic residue [64]. TRPM7 has a class II motif that is extremely conserved across species (human, mouse: S-V-R-L-M-L; Xenopus: S-L-R-L-M-L). This conserved motif suggested to us that TRPM7 may bind and be regulated by or through PDZ-containing scaffold proteins.

NHERFs are the best-studied PDZ-containing proteins expressed in epithelial cells. They play important roles in maintaining and regulating epithelial cell function. Expression studies have shown that the four members of the NHERF family are differentially and widely expressed [65, 66]. It seems that NHERF1 and NHERF2 are the most broadly distributed and abundantly expressed. NHERF1 is expressed highly in kidney, gastrointestinal tract, and liver. It is additionally found in the placenta, breast and brain. NHERF2 has a different spatial expressing pattern than NHERF1, with the highest expression level in lung. NHERF2 is also co-expressed in kidney with NHERF1, but with a distinct distribution pattern. In kidney, NHERF1 is expressed in proximal tubule while

NHERF2 localized to glomeruli and in collecting duct but not in proximal convoluted tubules. In addition, NHERF1 and NHERF2 were found mutually exclusively expressed in murine tissue. NHERF3 has similar tissue distribution to NHERF1 and NHERF2. It is expressed in the brush-border of epithelial cells in the kidney proximal tubules and the small intestine and also in liver. NHERF4 exhibits the most restricted tissue distribution of all the NHERFs, being found only in the gastrointestinal tract and kidney [65].

Investigations into the function of NHERF family members in mammals have revealed that NHERFs regulate the trafficking, localization and activity of ion channels and transporters as well as providing a physical link to the receptors that regulate their functions. More than 60 proteins targets have been identified for NHERF proteins, including transporters and ion channels, signaling proteins, hormone receptors and so forth [65, 67]. For example, NHERF proteins contribute critically to many G protein-coupled receptors (GPCR) mediated cell-specific signaling and function. Mahon et al showed that NHERF1 regulate PTH-mediated (parathyroid hormone-mediated) inhibition of inorganic phosphate uptake by a sodium-dependent phosphate transporter, Npt2a in OK cells (a proximal tubule-like opossum kidney cell line) [68]. NHERF1's first PDZ domain interacts with the last four amino acid of Npt2a and its COOH-terminus MERM domain binds to the cytoskeletal protein, ezrin. Therefore, NHERF1 serves as a membrane retention signal for Npt2a. PTH treatment of OK cells activates PTH1 receptor-mediated PKA and PLC pathways and results in the dissociation of Npt2a/NHERF1 complexes, which inhibits the phosphate transport by facilitating endocytosis of Npt2a. Thus, the fact that TRPM7 has a PDZ-binding motif and was found to interact with NHERF3 and NHERF in yeast-two hybrid screen suggests that NHERF proteins could be involved in the regulation of the channel.

5. Rationale and hypothesis

As the second most abundant intracellular cation, magnesium is involved in over 600 enzymatic reactions including energy metabolism and protein synthesis, and it also plays a pivotal role in human health and disease [69]. Over the past decades, the clinical relevance and biological significance of Mg^{2+} have attracted more and more attention. Mg^{2+} deficiency can be identified in up to 60% of critical ill patients and contributes to many human diseases and conditions, including hypertension, cardiac arrhythmias, atherosclerosis, and hypomagnesemia itself is considered to be especially harmful to fetuses and newborns [70-75]. At the physiological level, Mg^{2+} is a pivotal factor for muscular contraction, bone formation and neuronal excitability [69]. Consequently, the Mg^{2+} level in body has to be tightly regulated via ion channels and transporters.

The kidney plays a crucial role in regulating the Mg^{2+} level in blood by reabsorbing 80~95% of the total plasma Mg^{2+} that is filtered through the glomerulus. The reabsorbing process principally takes place within the nephron of the kidney (Figure 3). As is shown in Figure 3, 10-25% Mg^{2+} reabsorption occurs in the proximal convoluted tubule (PCT) and 50-70% of filtered Mg^{2+} is reabsorbed in the thick ascending limb of Henle's loop (TAL). However, the final Mg^{2+} level in the blood is determined at the distal convoluted tubule (DCT), since no reabsorption occurs beyond this this segment [69]. The responsible modulators and pathways controlling Mg^{2+} reabsorption in TAL and DCT have been established [76]. Several members from Claudin family (Claudin 16/19 and Claudin 14) play a prominent role in Mg^{2+} transport in TAL, while in DCT, the TRPM6 ion channel is thought to solely function in the kidney's distal tubule. However, the molecular mediator of Mg^{2+} reabsorption in proximal tubule has not yet been identified. A major driving force behind our studies is the gap in our understanding of TRPM7's function in proximal tubule,

where the channel is highly expressed. Does it mediate Mg^{2+} reabsorption in the proximal tubule, or does TRPM7 have other roles?

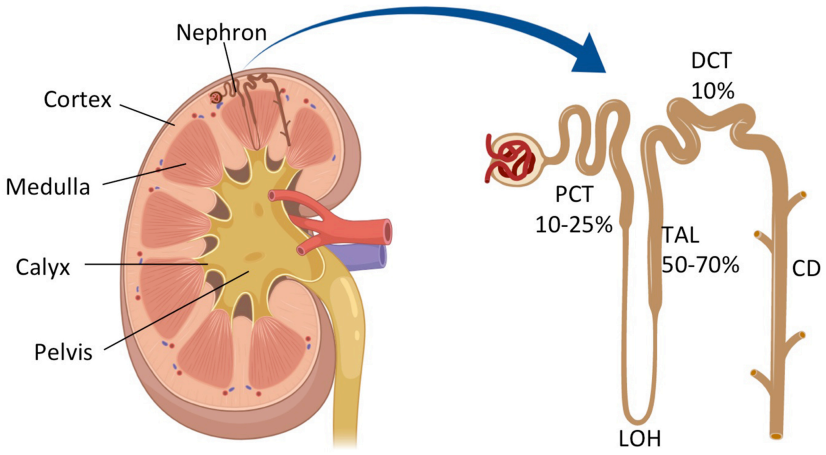

Figure 3. Magnesium handling in the nephron of kidney

The kidney plays a crucial role in regulating the Mg^{2+} level in human body by the reabsorption of Mg^{2+} filtered through the glomerulus. The nephron is the functional units of kidney. In the nephrons, 10-25% Mg^{2+} reabsorption happens in the proximal convoluted tubule (PCT), 50-70% of filtered Mg^{2+} is reabsorbed in the thick ascending limb of Henle's loop (TAL). However, the fine Mg^{2+} level is determined in the distal convoluted tubule (DCT), since no reabsorption of Mg^{2+} happens beyond this this segment.

Consequently, the aims of this study were to determine the function of TRPM7 in the renal proximal tubule, and to investigate the mechanism by which TRPM7 is controlled in proximal tubule cells. Specifically, our research was focused on understanding whether NHERF3 and NHERF4, which we identified as potential TRPM7 binding proteins from a yeast two-hybrid screen, played a role in channel regulation. Based on the observation by Shenolikar and colleagues that knockout of NHERF1 from mouse proximal tubule causes Mg^{2+} wasting in urine [77], and that NHERF1 and its binding partner NHERF3 are exclusively expressed in the proximal tubule, we speculated that loss of NHERF1 may have disrupted TRPM7's localization and function in the apical membrane of proximal tubule epithelial cells. Thus, based on our own research findings and evidence from the literature, we hypothesized that TRPM7 controls Mg^{2+} reabsorption in the proximal tubule and that the channels' localization to apical membranes is controlled by NHERF proteins (Figure 4).

Below we describe the results of our investigation. Our hope is that our research studies of the function and regulation of this Mg^{2+}-permeable channel will lead to novel approaches to minimize the impact of TRPM7 dysfunction on public health.

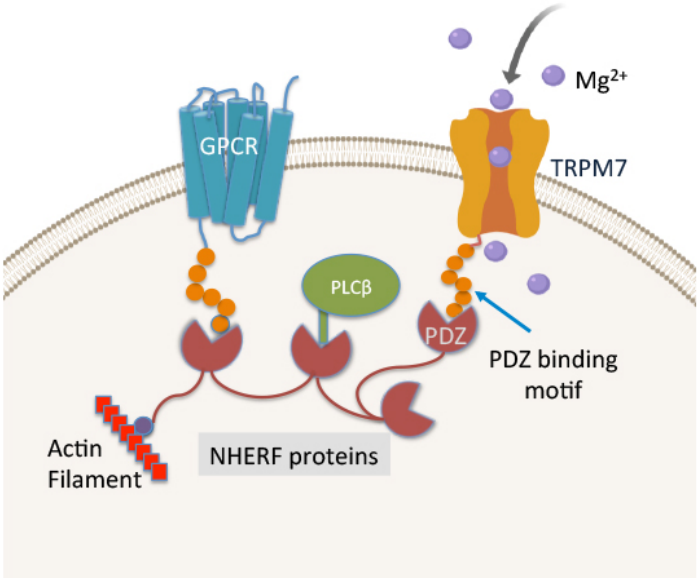

.

Figure 4. Working Model of TRPM7 function and regulation in mouse renal proximal tubule

We hypothesize that TRPM7 controls Mg^{2+} reabsorption in the proximal tubule and the channels localization to apical membranes is controlled its PDZ-binding motif to PDZ-domain containing NHERF proteins.

MATERIALS AND METHODS

1. Reagents

All of the cell culture reagents, unless otherwise stated, were purchased from Life Technologies (Carlsbad, CA). All of the chemicals, unless otherwise stated, were purchased from Sigma Aldrich (St. Louis, MO). Tetracycline, carbenicillin, kanamycin, were purchased from Gold Biotechnology (St. Louis, MO).

2. Animal studies.

All animal procedures were carried out in accordance with the approved guidelines. The procedures were approved by the Instructional Animal Care and Use Committee (IACUC) at Rutgers Robert Wood Johnson Medical School (Protocol #17-037).

3. Construction of mice with *Trpm7* knockout in proximal tubule by Cre-Lox recombination.

To generate *trpm7* knockout in renal proximal tubule mice, Trpm7$^{flox/flox}$ female mice were crossed with two strains of proximal tubule specific Cre male mice, gGT-Cre (γ-glutamyl transferase-cre), and PEPCK-Cre (phosphoenolpyruvate carboxylkinase), respectively. Trpm7$^{flox/flox}$ female mice were provided by Dr. David Clapham (HHMI) [49]. In the transgenic Trpm7$^{flox/flox}$ mice, the mutant locus harbors two LoxP sites flanking exon 17 of *Trpm7*. gGT-Cre and PEPCK-Cre mice were obtained from Vanderbilt University Kidney Disease Center. In both Cre lines, Cre-recombinase is expressed in renal cortex, where the proximal tubule is located [78]. For gGT-Cre mice five rounds of back crossing with C57BL/6 mice were performed.

4. Mouse strains and genotyping procedures

Mice were genotyped by PCR analysis of genomic DNA isolated from tail fragment, using a kit from Promega (Madison, WI). For analysis of genomic changes in the proximal tubule, roughly 20 μg of mouse kidney tissue was incubated in 600 μL of EDTA/Nuclei Lysis Solution (120 μL EDTA added to 500 μL Nuclei Lysis Solution, item# A794A, Promega, WI) containing 10-15 μL of 20 mg/mL Proteinase K (item# P8107S, New England Biolabs, MA) overnight at 55 °C. Samples were vortexed vigorously to ensure that the tissues were dissolved completely in the buffer. 200 μL of Protein Precipitation Solution (item# A795A, Promega, WI) was added to each sample to remove the proteins in the sample by centrifugation (11,000 rpm for 4 min). Next, the supernatants containing the DNA were carefully removed to another microcentrifuge tube containing 600 μL isopropanol to precipitate DNA. The DNAs were collected as a small white pellet by centrifugation (14,000 rpm for 1 min). The DNA pellet was washed with 600 μL 70% of ethanol and collected by centrifugation at 14,000 rpm for 1 min. 100 μL of DNA Rehydration Solution (item# A796A, Promega, WI) was added to rehydrate the DNA by incubating the solution overnight at 4 °C. The obtained genomic DNAs were subjected to PCR reaction for genotype analysis. The primers and PCR conditions are listed in Appendix Table 2.

5. Housing and metabolic profiling of mice.

Mice were kept on 12/12-hour light/dark cycle and allowed *ad libitum* to food and water. Litters were weaned at three weeks of age and genotyped by PCR. For the dietary Mg^{2+} deprivation experiments, *trpm7 KO* and control mice were fed with Mg^{2+}-deficient chow containing 0.003% Mg^{2+}. Blood samples were taken from submandibular vein of mice and then processed as follows. The serum was incubated for 1 h at room temperature. Next,

clots were removed by centrifugation (2,000 rpm for 30 min at room temperature) and the serum supernatant was reserved and stored frozen at -80°C. To obtain urine samples, mice were maintained for 24 h in individual metabolic cages under housing conditions as described above. Urine samples were collected after 24 h and stored at -80°C. Content of Mg^{2+} in both serum and urine samples was determined using the Magnesium Assay Kit (Sigma-Aldrich). The total amount of urinary excretion of Mg^{2+} in 24 h was calculated by multiplying measured Mg^{2+} concentration times the collected urine volume.

6. Mg^{2+} measurements in mouse biological samples

Mg^{2+} concentrations in mouse urine and serum samples were determined using Magnesium Assay Kit (Sigma-Aldrich, MO), according to the manufacturer's protocol. The coupled enzyme assay exploits the specific requirement of glycerol kinase for Mg^{2+}, resulting in a colorimetric product proportional to the amount of magnesium present.

To a clear 96-well flat-bottom plate, 3 µL serum samples or 2 µL 1:20 diluted urine was added. The final volume of the samples was brought up to 50 µL with double distilled water. In the same plate, a series dilution of magnesium standard provided by manufacturer was used to generate a standard curve to calculate magnesium concentrations. For the enzymatic assay, 50 µL of the reaction mix containing 35 µL magnesium assay buffer, 10 µL color developer and 5 µL magnesium enzyme mix were added to the prepared samples and the standards. The reaction mixtures were mixed well, using horizontal shaker and incubated for 10 minutes at 37 °C. The absorbance was then measured at 450 nm by Spectrophotometric multiwall plate reader (SpectraMax M2, Molecular Devices) as A_{450}. The reactions were continued to incubate at 37 °C taking measurement (A_{450}) every 5 minutes until the final A_{450} reached 1.5. The amounts of magnesium contained in the samples were determined from the standard curve that was generated by the magnesium

standard provided by manufacturer. The concentration of magnesium in sample was calculated by the formula:

$C = S_a/S_v$

C = Concentration of magnesium in sample

S_a = Amount of magnesium in unknown sample (nmol)

S_v = Sample volume (μL) added to reaction well

7. Hematoxylin & Eosin (H&E) analysis

Kidneys were dissected from anesthetized mice and fixed overnight with 4% (vol/vol) paraformaldehyde (PFA) in PBS at 4°C for paraffin-embedded sections. Paraffin-embedded sections were stained with H&E at the Biospecimen Repository Service Center of Cancer Institute of New Jersey. To briefly describe the H&E procedure, the formalin-fixed paraffin-embedded (FFPE) tissue were cut onto slides and is baked at 60 °C for 1 h. The slides were then cooled and placed onto a staining rack and then on the automatic Tissue Tek H&E stainer and a tonsil control slide is added. The staining sequence is as follows:

- 3 changes of xylene for deparaffinization (4 min each)
- 2 changes of 100% ETOH for removal of xylene (1 min each)
- 1 change of 95% ETOH to start hydration (1 min each)
- 1 change of 70% ETOH for hydration (1 min each)
- 2 changes of water to remove all ETOH (1 min each)
- Hematoxylin (8 minutes)
- 1 change of water (2 min)
- 1 change of Acid Alcohol (30 seconds, as Hematoxylin is a regressive stain)

- 1 change in tap water (2 min)
- Bluing Agent (2 min., to deepen the blue color of nuclei)
- 1 change of water (2 min)
- 1 change of 95 ETOH 30 seconds., to prepare for Eosin)
- Eosin (2 minutes)
- 4 changes of 100% ETOH (2 min each)
- 3 changes of xylene (2 min each)

Slide rack was then placed onto the automatic coverslipper to finish.

8. Transmission electron microscopy

For the transmission electron microscopy study, we dissected kidneys from anesthetized *trpm7* KO and WT mice using the midline abdominal incision. The cortex of the dissected kidneys was sliced off carefully and cut into 1 mm square samples. The samples were then fixed using 2.5% glutaraldehyde mixed with 4 % paraformaldehyde in 0.1 M cacodylate buffer, followed by a post-fixation in buffered 1% osmium tetroxide. The samples were subsequently dehydrated in a graded series of acetone and embedded in Embed812 resin. About 90 nm thin sections were sliced using a Leica UC6 ultramicrotome and then stained with saturated solution of uranyl acetate and lead citrate. Images were captured with an AMT (Advanced Microscopy Techniques) XR111 digital camera at 80 Kv on a Philips CM12 transmission electron microscope.

9. Statistical analysis

Student's *t*-test and ANOVA methods were used to calculate p values based on comparisons with the appropriate control samples tested at the same condition. *p* values <0.05 (*) were considered statistically significant.

10. DNA constructs

The pcDNA5/FRT/TO-HA-mTRPM7 (HA-TRPM7) was generated in earlier studies [24, 79]. pcDNA5/FRT/TO-HA-mTRPM7ΔPDZ (HA-TRPM7ΔPDZ) mutant construct was generated using the Quickchange mutagenesis kit (Stratagene, CA). Flag-tagged human NHERF1 plasmid was obtained from Addgene (Watertown, MA, plasmid# 28291). Flag-tagged NHERF2 and NHERF4 were constructed by subcloning the human NHERF2 and NHERF4 plasmid purchased from Addgene (plasmid# 28292 and 38880) into pcDNA6/V5/-HisB vector. The pcDNA3.1/hygro-FLAG-NHERF3 was provided by Dr. Allan Wolkoff from Albert Einstein College of Medicine. The primers for creating these constructs were summarized in Appendix 1.

11. Cell culture and transfection

The 293T cell line (CRL-3216) was purchased from American Type Culture Collection (ATCC, Manassas, VA). The tetracycline inducible HEK-293-TRPM7 and HEK-293-TRPM7Δ6 stable cell lines were generated using the Flp-In system (Thermofisher, CA), using the commercially available Flp-In T-Rex 293 cells as described in a previous study [24]. To make above cell lines, pcDNA5/FRT/TO-HA-TRPM7, which expresses N-terminal hemagglutinin (HA)-tagged murine TRPM7, or pcDNA5/FRT/TO-HA-

TRPM7Δ6, was co-transfected with the plasmid expressing Flp recombinase (pOG44) together into the parental cell line. Hygromycin was employed for clonal selection.

The HEK293T, HEK293-HA-TRPM7 and HEK293-HA-TRPM7Δ6 cells were all maintained in a Dulbecco's Modified Eagle Medium (DMEM), high glucose media containing 10% fetal bovine serum (Atlanta Biologicals, GA) and 1% L-glutamine in a humidified 37°C, 5% CO2 incubator. Transient transfections in these cell lines were performed using the Turbofect transfection reagent (Thermo Fisher, MA), according to the manufacturer's protocol.

The Opossum kidney proximal tubule (OK) cell line was provided by Dr. Judith A. Cole from Department of Biological Sciences, the University of Memphis. The cells were cultured in DMED/F12 medium supplemented with 5% of FBS. Transfection of OK cells were carried out using Lipofectamine3000 (Thermo Fisher, MA), according to the manufacturer's protocol.

12. Mass spectrometric analysis of TRPM7 immunopurified from OK cells

To identify the cell-cell adhesion proteins that interact with TRPM7 in OK cells, we used anti-HA agarose beads to immunoprecipitate HA-TRPM7, which was transiently expressed in OK cells for 48 hours. Specifically, 2 x 10^6 OK cells were seeded onto 10 cm dish. 10 µg of HA-TRPM7 plasmid was transfected in the cells the next day. Cell lysates were collected in 1 mL mild lysis buffer containing protease inhibitor cocktail (Roche Life Sciences, IN) containing phosphatase inhibitor cocktail (EMD Millipore, Germany) and subjected to immunoprecipitation by 20 µl HA-agarose (Sigma-Aldrich, MO) overnight at 4°C. The immunoprecipitated protein complex were resolved in a 10% Bis-Tris

polyacrylamide gel. Protein bands were visualized by Coomassie blue staining and excised from the gel for Mass Spectrometry analysis at the Biological Mass Spectrometry Facility at Rutgers Robert Wood Johnson Medical School.

13. Immunocytochemistry

1 x 10^5 OK cells were seeded onto glass coverslips placed into 24-well plates 24 h before transfection was performed. To study the localization of TRPM7 and TRPM7Δ6, OK cells were transfected with 0.4 μg HA-TRPM7 or 0.4 μg HA-TRPM7Δ6. To study the co-localization of TRPM7 and other proteins, including as myc-tagged plakoglobin, GFP-tagged desmoplakin or NHERF proteins, cells were co-transfected with 0.4 μg HA-TRPM7 and 0.4 μg of other plasmids, plakoglobin-myc (Addgene, Watertown, MA), desmoplakin-GFP (Addgene, Watertown, MA) or NHERF proteins. 48 h post-transfection, cells were fixed using 4% paraformaldehyde in PBS for 20 min at room temperature. 0.1% Triton X-100 in PBS were used to permeabilized the cells at 30 °C for 10 min and then 5% FBS in PBS were used for blocking at 30 °C for 30 min. Then cells were incubated in appropriate primary antibodies for 1 h at 30 °C. To detect HA-TRPM7 and HA-TRPM7Δ6, we used a rat monoclonal antibody anti-HA antibody (3F10; Roche Life Sciences, IN) (1:1000 dilution). To detect plakoglobin and desmoplakin, we used anti-Myc and anti-GFP antibodies from Santa Cruz (1:500, Santa Cruz Biotechnology, Inc., TX). For NHERF proteins, we employed the anti-FLAG antibody from Sigma Aldrich (1:2000). After three 5-min washing steps with 5% FBS in PBS, Alexa Fluor™ 488 and Alexa Fluor™ 568 were used as secondary antibodies (Thermo Fisher, MA) (1:2000 dilution). then followed by 5-min incubation of DAPI (1:4000 dilution) at 30 °C. After 3 washes with 5% FBS in PBS and 3 washes with PBS, the coverslips with cells were mounted onto glass slide with Aqua

Poly/Mount (Polyscience, Inc). Images were taken by a Yokogawa CSUX1-5000 microscope under 63X magnification using 488 nm and 561 nm wavelengths at the Rutgers RWJMS CORE Confocal facility.

14. Investigation of the effect of TRPM7's channel on E-cadherin expression and localization

1 x 10^5 OK cells were seeded on glass coverslips in 24-well plates for 72 h to allow time for cell-cell adhesion formation. To inhibit TRPM7's channel activity, cells were treated with 30 μm NS8593 hydrochloride (Tocris Bioscience, Minneapolis, MN) for 5 h. To activate TRPM7's channel activity, cells were incubated with 20 μm Naltriben mesylate (Tocris Bioscience, Minneapolis, MN) for 5 h. After incubation, cells were then fixed and subjected to immunocytochemical analysis. The effect of adding the TRPM7 channel modulators on E-cadherin localization was determined by analyzing the change of the localization of endogenous E-cadherin using an E-cadherin antibody (BD Transduction Laboratories, Lexington, KY).

15. Co-immunoprecipitation of TRPM7 and NHERF3

Approximately 1.0 x 10^6 HEK-293T cells were seeded onto a 60 mm dish. 2.5 μg of HA-TRPM7 plasmid was co-transfected with 2.5 μg of FLAG-NHERF3 in the cells the next day. After 48 h of expression, cell lysates were collected in 1 mL mild lysis buffer containing protease inhibitor cocktail (Roche Life Sciences, IN) and phosphatase inhibitor cocktail (EMD Millipore, Germany. HA-TRPM7 was immunoprecipitated using 20 μl HA-agarose (Sigma-Aldrich, MO) overnight at 4°C. Lysates input (20 μl) and IP samples were separated by SDS-PAGE and proteins were detected by immunoblotting. The rabbit

polyclonal anti-TRPM7 antibody (Anti-C47) was used to detect HA-TRPM7, and a mouse anti-FLAG antibody was used to detect FLAG-NHERF3.

16. *In Vitro* GST pull-down purification assay

Pull-down purification assays were conducted using recombinant proteins fused to GST. GST fusion proteins were expressed in *E. coli* BL21-DE3 cells (Agilent Technologies, CA). Bacteria in 250 mL cultures were grown at 37°C to reach OD600 of 0.7-1.0 and then induced with 1 mM isopropyl isopropyl-β-D-1-thiogalactopyranoside (IPTG, Gold Biotechnology, MO) for 4 h at 37°C. Bacterial cells were collected by centrifugation. The bacteria pellet was re-suspended and lysed by sonication in 10 mL of ice-cold PBS containing 1% Triton-X100 (PBST). The cell lysates were then incubated with 500 μL glutathione agarose beads with rotation for 2~3h at 4°C. Then the agarose beads were washed with 10 mL PBST buffer three times at 4°C. The concentrations of GST fusion proteins for pulldown assay were evaluated by resolving the proteins on an 15% SDS-PAGE gel and compare the protein levels by Coomassie staining.

For GST pulldown assays, approximately 0.3 x 10^6 HEK293T cells were plated on 10 cm culture dishes overnight. 10 μg of plasmids were transiently transfected into the 70%-confluent HEK293T cells and the proteins were allowed to express for 24 h. Cell lysates were harvested using 1 mL lysis buffer containing protease inhibitor cocktail (1:100, Roche Life Sciences, IN) and incubated with 20 μL GST fusion proteins bound on glutathione agarose for overnight by rotation at 4°C. Cell lysate input (20 μl) and GST pulldown samples were heated at 95 °C to elute the proteins from glutathione beads. The eluted proteins were then separated by SGS-PAGE and analyzed by Western blot analysis. An anti-Flag antibody from Sigma was used to detect Flag-tagged NHERF proteins, and

an anti-GFP antibody (sc-9996; Santa Cruz Biotechnology, Inc., TX) was used to detect GFP-TRPM7-Cterm.

17. Immunoblotting

Cells treated with the conditions indicated were washed with ice-cold PBS and lysed with 200~500 μL mild lysis buffer (50 mM Tris (pH 7.4), 150 mM NaCl, 1% IGEPAL CA-630 containing protease inhibitor cocktail). The lysates were then incubated at 4°C with rotation for 0.5 h to solubilize TRPM7 from membranes. After incubation, the lysates were then centrifuged at 14,000 rpm for 10 min at 4°C. For Western blot, the supernatant fractions were subjected to SDS-PAGE and transferred to a PVDF membrane (BioRad Laboratories, CA). The membranes were blocked with 5% nonfat milk in PBST for 0.5 h at room temperature. Afterwards, the blot was incubated with appropriate primary antibodies at 4°C overnight. A secondary antibody linked to horseradish peroxidase was used at a dilution of 1:5000 for 2 h at room temperature. Specific signals were visualized by enhanced chemiluminescence (ThermoScientific, IL).

18. Electrophysiology

Whole cell TRPM7 and TRPM7Δ6 currents were recorded by Axopatch 200B (Axon Instruments, Inc) equipped with Low-Noise Data Acquisition System Digidata1440A (Molecular Devises), as previously described [3]. Tetracycline was added to TRPM7 and TRPM7Δ6 stable cell lines to induce protein expression. Electrophysiological measurements were performed 24 h after induction. Whole cell currents were elicited by voltage stimuli lasting 250 ms and delivered at 1s intervals, with voltage ramps ranging from -100 to +100 mv. Data were digitized at 2 or 5 kHz, and digitally filtered off-line at 1 kHz. The internal pipette solution (intracellular solution) contains: 145 mM Cesium

methanesulfonate ($CsSO_3CH_3$), 8 mM NaCl, 10 mMEGTA, and 10 mM HEPES, with pH adjusted to 7.2 with CsOH. The osmolarity of intracellular solution was adjusted to be 280-290 osmol/L. Ca^{2+} was adjusted to various concentrations using MaxChelator. The standard extracellular Tyrode's solution for whole cell recording contains: 145 mM NaCl, 5 mM KCl, 2 mM $CaCl_2$, 10 mM HEPES and 10 mM glucose, with pH adjusted to 7.4 with NaOH. MaxChelator was used to calculate free Ca^{2+} and free Mg^{2+} concentration. The osmolarity of extracellular solution was adjusted to be 310-320 osmol/L.

19. Manipulation of the PKC activity in OK Cells

1 x 10^5 OK cells were seeded on glass coverslips in 24-well plates for 24 h before transfection were performed. Each well of cells were transfected with 0.4 μg HA-TRPM7 or co-transfected with 0.4 μg HA-TRPM7 and 0.4 μg Flag-tagged NHERF proteins. After 48 h, the transfected cells were incubated either with 2 μM Cheryl chloride for 6 ~ 24 h to inhibit PKC or with 20 nM Phorbol 12-myristate 13-acetate (PMA) for 2 h to activate PKC. The treated cells were then fixed using 4% paraformaldehyde in PBS and subjected to immunocytochemical analysis.

EXPERIMENTAL RESULTS

SECTION I: Deletion of TRPM7 in Renal Proximal Tubule Causes Growth Retardation and Cyst Generation in Mouse Kidney

1.1 Deletion of *Trpm7* in renal proximal tubule causes growth retardation in mouse

To examine the function of TRPM7 in mouse kidney proximal tubule, we created two strains of *trpm7* knockout mice in proximal tubule by crossing conditional female $Trpm7^{flox/flox}$ mice (gift of David Clapham, HHMI) with either male PEPCK-Cre (phosphoenolpyruvate carboxylkinase) or gGT-Cre (γ-glutamyl transferase-cre) mouse (Figure 5A). The exon 17 in $Trpm7^{flox/flox}$ was flanked by LoxP sites. In the tissues where Cre expressed, exon 17 is eliminated by Cre-Lox recombination, which would lead to complete loss of function of TRPM7 channel-kinase [49]. PEPCK is the enzyme that catalyzes the first step of gluconeogenesis converting oxaloacetate to phosphoenolpyruvate and is dominantly expressed in periportal hepatocytes and in renal proximal tubules [80, 81]. The PEPCK-Cre transgenic mouse was constructed using a modified version of the original PEPCK promotor, in which the PEPCK expression was reduced by 60% in liver and increased by 10-fold in the kidney [82]. For the gGT-Cre strain, there were 3 variants of rat γ-glutamyl transpeptidase mRNAs (Type I, II and III), which were identified to have difference 5' untranslated sequence but produce identical gGT proteins [83] . The type I mRNA has been shown to be expressed in almost exclusively in the proximal tubules of fetal or adult kidneys [84]. The gGT-Cre transgenic mouse used in our study was carrying the Cre recombinase gene driven by the gGT promotor I [78].

The deletion of *Trpm7* in renal proximal tubule in these two strains of transgenic mouse was confirmed by PCR analysis. The representative genotyping results using the

kidney cortex tissue of the control *Trpm7*$^{flox/flox}$ mice and *trpm7 KO* mice are shown in Figure 5B.

A

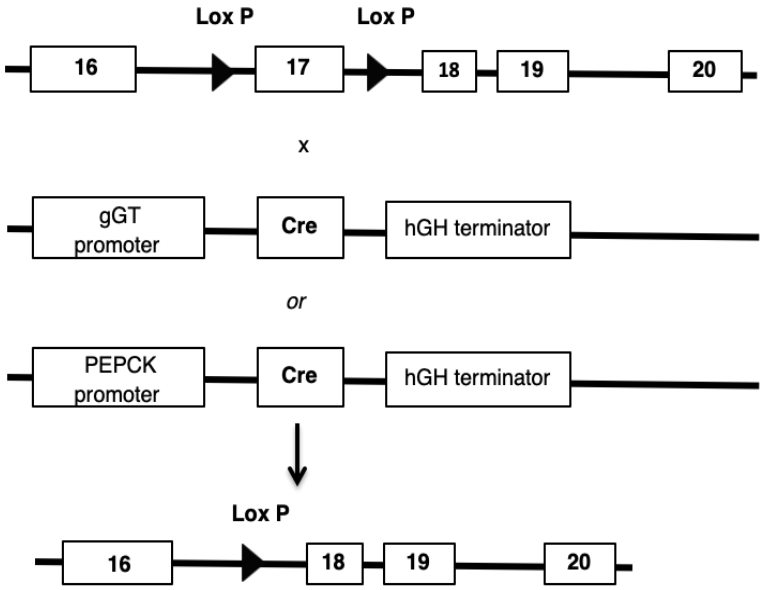

B

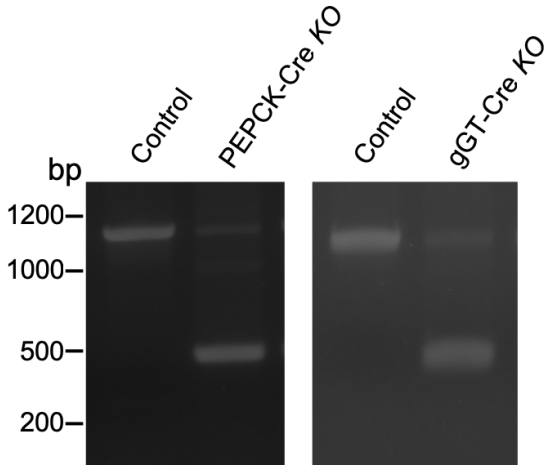

Figure 5. Conditional deletion of TRPM7 and genotypic analysis

(A) The strategy of homologous recombination for the tissue-specific *trpm7* knockout in the proximal tubule of mouse. The exon 17 in Trpm7$^{flox/flox}$ was flanked by LoxP sites. In the tissues that have Cre expressed, exon 17 is eliminated by Cre-Lox recombination, which would lead to complete loss of function of TRPM7 channel-kinase. **(B)** Identification of the mouse genotype by PCR analysis of a kidney cortex tissue-derived DNA. The PCR product in the upper gel showed the presence of exon 17 within the *Trpm7*$^{flox/flox}$ allele. The lower band showed the deletion of exon 17 segment by Cre recombinase.

The PEPCK-Cre *KO trpm7* mice didn't show conspicuous abnormalities in morphology and behavior. However, the deletion of *Trpm7* by gGT-Cre in renal proximal tubule was found to have severe effects on the female *trpm7 KO* pups. About 20% (n = 19) of female *KO* pups were born with much smaller body size than their littermates and were much less physically active compared to their floxed littermates. The small female *trpm7* KO pups often died before 6 weeks of age. Figure 6 showed an example of the difference between these *trpm7 KO* pups and their control littermates in terms of their body size and appearance. The 5-week-old mutant pup only weighted about 1/3 of its control littermate (4.5 g vs. 15.3 g, Figure 6A). The fur of the *KO* pup was thinner than the control littermate and the paws of the *KO* pup were much paler compared to the healthy-looking pink color of its control littermate's paws (Figure 6B). In addition, we also observed that the mutant pups that were housed in the same cage with their littermates always appeared much weaker and were much less physically active than their littermates, even though they were maintained under the same condition.

A

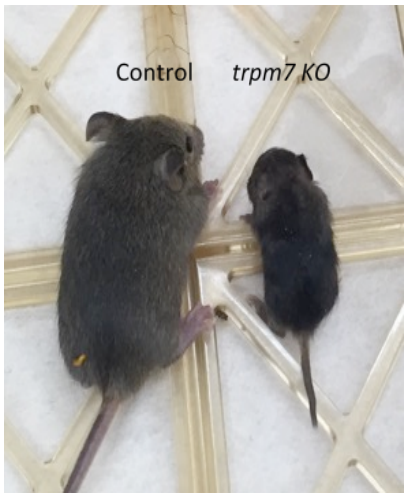

B

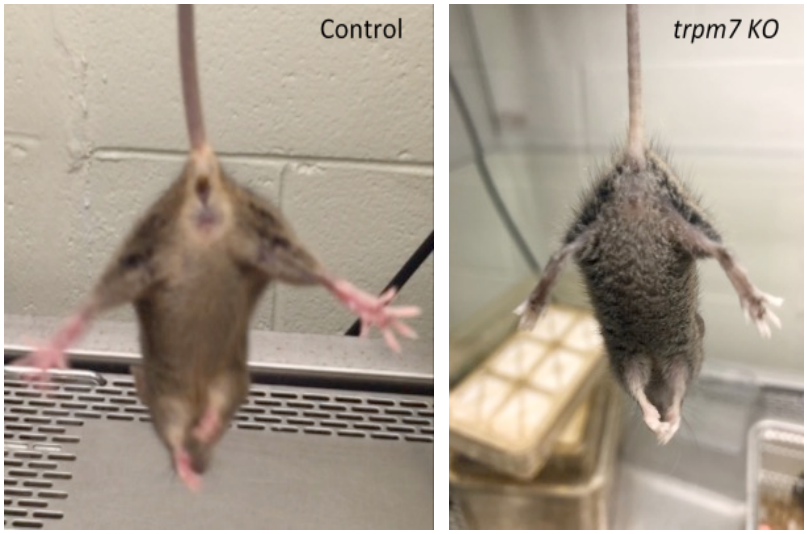

Figure 6. Representative images of a gGT-Cre *KO trpm7* young pup and its control littermate.

(A) A representative image showing the severe phenotype of the TRPM7-deficient pup, which had much smaller body size compared to its control littermate. **(B)** Representative images comparing the appearance TRPM7-deficient pup with its control littermate. The deficient pup had thinner fur and paler paws comparing with its control littermate. Both *KO* and control mice were 5-week-old females.

Among those pups that survived over 2 months, the disruption of *Trpm7* was found to cause growth defects in the mutant mice. For the PEPCK-Cre *KO trpm7* strain, only the female *trpm7 KO*, but not the male *trpm7 KO*, showed significant decrease in body weight compared to the control group (Figure 7A and 7B). For *trpm7 KO* by gGT-Cre mice, both male and female *trpm7*$^{-/-}$ mice were significantly lighter than their control littermates (Figure 7C and 7D). These different observations between two *trpm7 KO* strains may be due to the differences in the efficiency of Cre-mediated knockout between gGT-Cre and PEPCK-Cre recombinase.

To confirm the growth-delayed phenotype of *trpm7*$^{-/-}$ mice, we followed the growth process of a group of female gGT-Cre *KO trpm7* mice and their littermates by measuring their body weights every 2-4 weeks from the age of 5 weeks to 24 weeks and found that the *trpm7 KO* mice were always lighter than their littermates through the whole growth process.

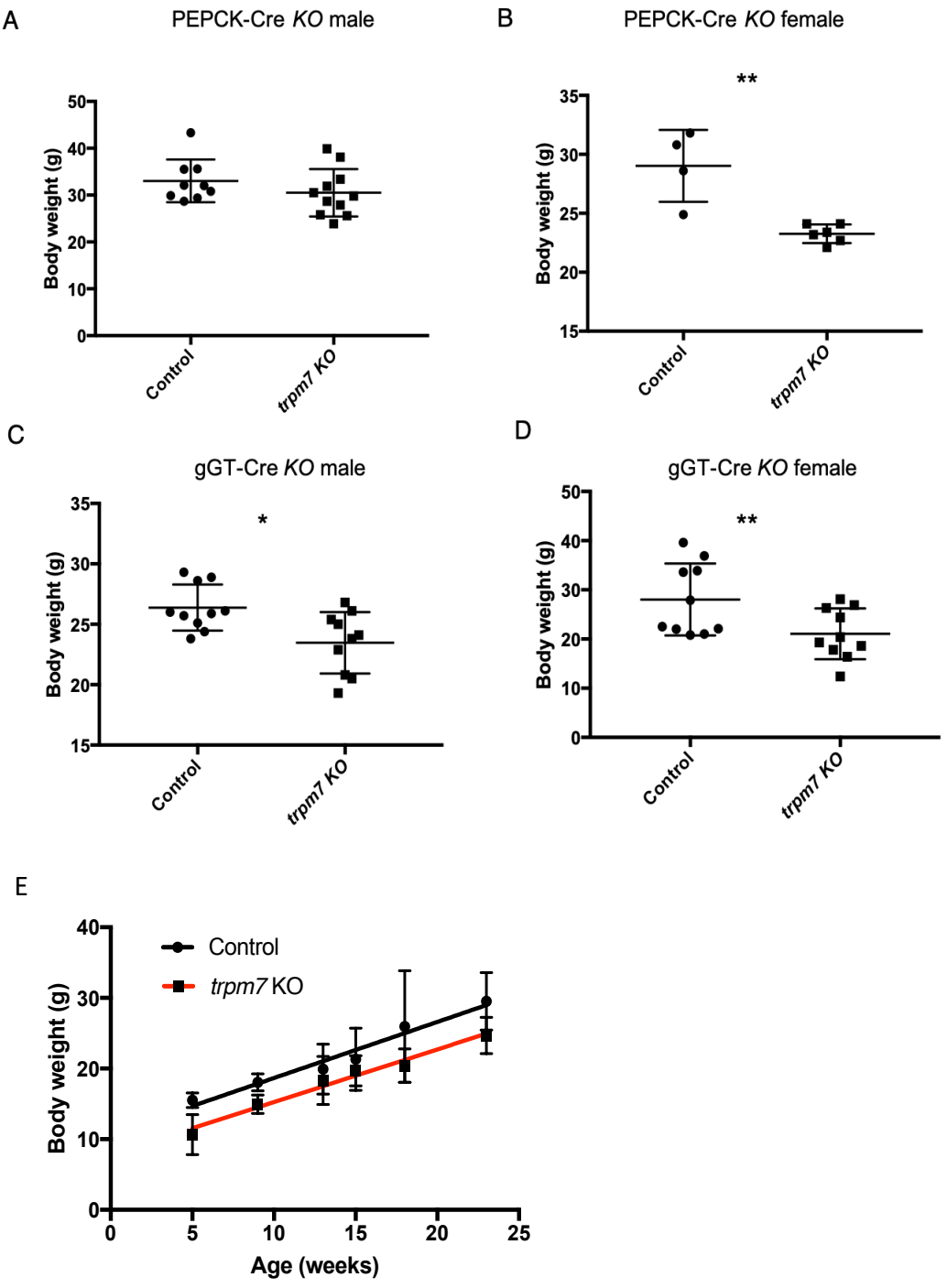

Figure 7. Disruption of *Trpm7* gene in proximal tubule causes a growth retardation phenotype

(A) The male PEPCK-Cre *KO trpm7* mice had similar body weight as their littermates. control (n = 9) and *trpm7 KO* (n = 11), $p = 0.26$. **(B)** The female PEPCK-Cre *KO trpm7* mice showed significantly lower body weight than their littermates. control (n = 4) and *trpm7 KO* (n = 6), $p < 0.01$. **(C)** The male gGT-Cre *KO trpm7* mice exhibited significantly lower body weight than their littermates. control (n = 10) and *trpm7 KO* (n = 10), $p < 0.05$. **(D)** The female gGT-Cre *KO trpm7* mice showed significantly lower body weight than their littermates. control (n = 10) and *trpm7 KO* (n = 10), $p < 0.01$ **(E)** The growth process of gGT-Cre *KO trpm7* mice was tracked by measuring the body weights of the mice constantly from the 5^{th} weeks to 24^{th} weeks. Compared to the control group, the *trpm7 KO* mice were always lighter than their control littermates throughout the whole growth stages (n = 4-6, $p < 0.01$). Two-tailed student *t* test was used for the statistical analysis. * $p < 0.05$, ** $p < 0.01$. All mice used in these experiments were 30~32-week-old.

1.2 Deletion of *Trpm7* in renal proximal tubule does not affect Mg^{2+} status of mice

Both of TRPM7 and its close homolog TRPM6 play an essential role in regulating the whole-body Mg^{2+} homeostasis. Disruption of *Trpm6* in distal convoluted tubule in humans causes hypomagnesemia with secondary hypocalcemia [58]. The proximal tubule is also an important compartment within the nephron for Mg^{2+} reabsorption, where about 20-30% of filtered Mg^{2+} is reclaimed [85]. However, the specific molecular mechanism by which magnesium is reabsorbed in proximal tubule remains unknown. Since TRPM7 was found to have high expression level in proximal tubule and is implicated in the regulation of Mg^{2+} homeostasis, we hypothesized that TRPM7 might play a role in regulating Mg^{2+} reabsorption in proximal tubule and the retarded growth phenotype we found in both *trpm7 KO* Cre strains could be due to Mg^{2+} deficiency.

To investigate the role of TRPM7 in Mg^{2+} reabsorption in proximal tubule, we evaluated the Mg^{2+} status in *trpm7 KO* mice by measuring the amount of Mg^{2+} excreted in urine and the Mg^{2+} level in blood serum. The results of the assessment of Mg^{2+} status in mice are summarized in Figure 8-11. Male and female individuals were examined separately as the Mg^{2+} metabolism in both genders are different [86].

The urinary excreted Mg^{2+} in PEPCK *trpm7 KO* mice showed no significant difference compared to that of their control littermates (Figure 8A, $p = 0.681$). Similarly, the Mg^{2+} level in the serum of the *trpm7 KO* animals were also found not to be significantly different from that of control littermates (Figure 8B, $p = 0.399$). Therefore, we did not find any evidence that the disruption of *Trpm7* in the proximal tubule using PEPCK-Cre recombinase affected Mg^{2+} homeostasis in male mice.

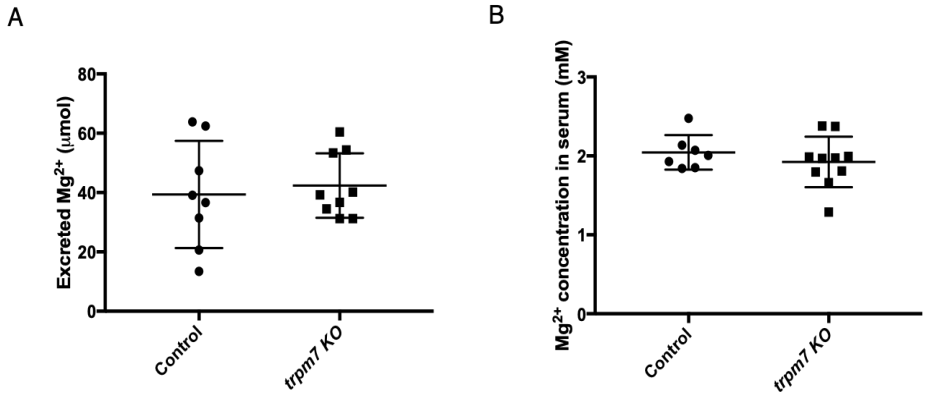

Figure 8. Disruption of *Trpm7* gene in proximal tubule by PEPCK-Cre recombinase did not alter the Mg^{2+} status in male *trpm7 KO* mice.

(A) Assessment of the amount of urinary excretion of Mg^{2+} in PEPCK-Cre *KO trpm7* (n = 9) and control (n = 8) mice, $p = 0.681$. **(B)** Assessment of the level of Mg^{2+} in the serum of male PEPCK-Cre KO *trpm7* (n = 10) and control (n = 7) mice, $p = 0.399$. Two-tailed student *t* test was used for the statistical analysis. $p < 0.05$ was considered significant. All mice in these experiments were 30-week-old male.

We speculated that differences in Mg^{2+}-handling between control and PEPCK-Cre *KO trpm7* mice might better be revealed under conditions of Mg^{2+}-deprivation [26]. To test this hypothesis, both of the control and PEPCK-Cre *trpm7 KO* mice were switched from PicoLab Mouse Diet 20 containing 0.17% Mg^{2+} to a Mg^{2+} deficient diet containing 0.003% of Mg^{2+}. After feeding the animals with low Mg^{2+} diet for 14 days, we placed the animals in metabolic cages to capture urine for Mg^{2+} assessment. Under Mg^{2+} deprivation condition, the amount of excreted Mg^{2+} in mouse urine reduced dramatically (from 40 to 6 μmol per day, Figure 9A). However, we did not observe significant difference in the amount of excreted Mg^{2+} between *trpm7 KO* and the control group. Mg^{2+} deprivation also altered the Mg^{2+} level in the serum of the mice (Figure 9B), the average Mg^{2+} concentration in mouse serum dropped from 2 to 0.8 mM. However, there was still no significant difference in the serum Mg^{2+} levels between the *trpm7 KO* group and control group, indicating that *trpm7 KO* mice did not exhibit a Mg^{2+} deficiency phenotype, even under the condition of Mg^{2+} deprivation.

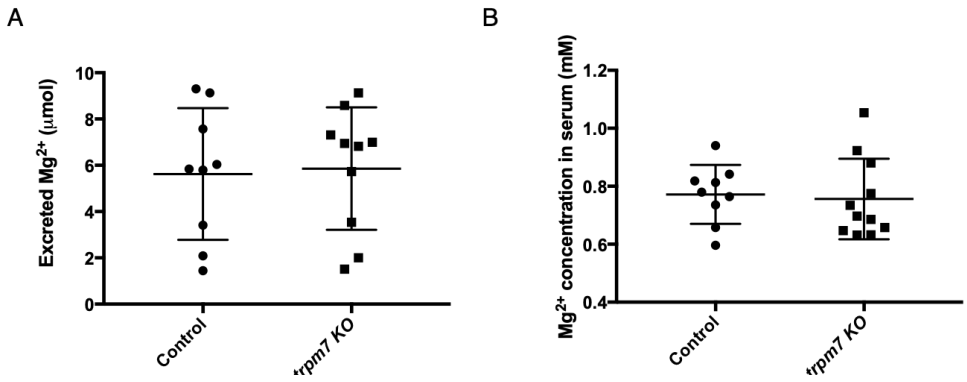

Figure 9. Male PEPCK-Cre KO trpm7 mice did not exhibit Mg^{2+} deficiency upon Mg^{2+} deprivation.

(A) Assessment of the urinary excretion of Mg^{2+} in PEPCK-Cre *KO trpm7* (n = 10) and control (n = 9) mice subjected to low Mg^{2+} diet for 14 days, $p = 0.855$. **(B)** Assessment of the level of Mg^{2+} in the serum of male PEPCK-Cre *KO trpm7* (n = 11) and control (n = 9) mice subjected to low Mg^{2+} diet for 14 days, $p = 0.781$. Two-tailed student *t* test was used for the statistical analysis. $p < 0.05$ was considered significant. All mice were 30-week-old males.

We separately evaluated the Mg^{2+} status of female PEPCK-Cre *KO trpm7* mice, given that the female animals have a different Mg^{2+} metabolism from male animals. The results of assessment of Mg^{2+} status in female PEPCK-Cre *KO trpm7* mice is shown in Figure 10. Female mice were found to excrete much less Mg^{2+} in 24 h compared to male mice (40 *vs.*20 μmol, Figure 10A). Compared to the control group, the *trpm7 KO* mice excreted slightly lower amounts of Mg^{2+}, but the reduction was not statistically significant (Figure 10A). Female mice exhibited lower level of Mg^{2+} in their blood serum compared to male mice (1.25 *vs.* 2 mM, Figure 10B). However, there was no significant difference being observed between *trpm7 KO* group and control group. Similarly, for the male mice, even being switched from the normal diet to Mg^{2+} deprivation diet, the female *trpm7 KO* mice failed to show any significant difference in either excreted Mg^{2+} or Mg^{2+} concentration in serum from the control group (Figure 10C and Figure 10D). However, it is worth noting that after being fed with Mg^{2+}-deficient diet for 14 days and housed in metabolic cage for 24 h, 3 animals died in the *trpm7 KO* group, while only 1 animal in the control group died, indicating that compared to the control mice, *trpm7 KO* mice may be more vulnerable to Mg^{2+} deprivation.

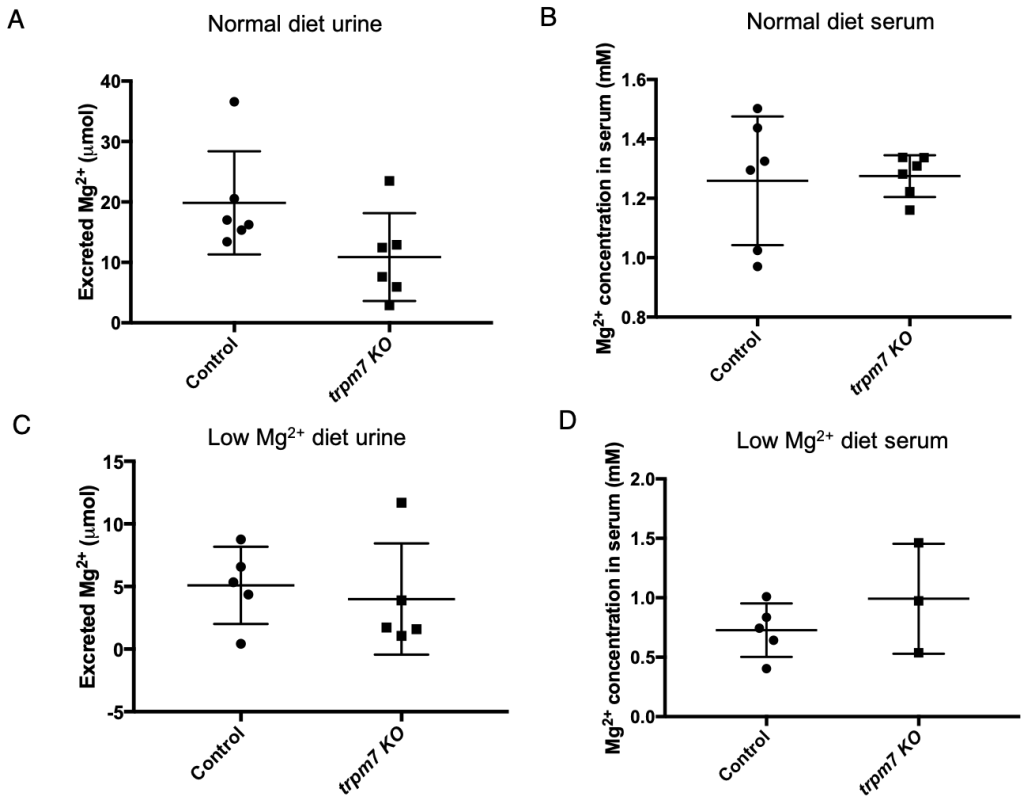

Figure 10. Assessment of the Mg^{2+} status in female PEPCK-Cre *KO trpm7* mice under normal and Mg^{2+} deprivation conditions.

(A) Comparison of the urinary excretion of Mg^{2+} in PEPCK-Cre KO *trpm7* (n = 6) and control (n = 6) mice, $p = 0.0784$. **(B)** Comparison of the level of Mg^{2+} in the serum of male PEPCK-Cre KO *trpm7* (n = 6) and control (n = 6) mice, $p = 0.869$. **(C)** Comparison of the urinary excretion of Mg^{2+} in 30-week-old male PEPCK-Cre KO *trpm7* (n = 5) and control (n = 5) mice on low Mg^{2+} diet, $p = 0.662$. **(D)** Comparison of the level of Mg^{2+} in the serum of male PEPCK-Cre KO *trpm7* (n = 5) and control (n = 3) mice on low Mg^{2+} diet, p =

0.408. Two-tailed student *t* test was used for the statistical analysis. $p < 0.05$ was considered significant. All mice in these experiments were 30~32-week-old female.

We then performed similar studies to analyze the Mg^{2+} status of gGT-Cre *KO trpm7* animals. The results for male *trpm7 KO* mice were shown in Figure 11A-11B. There was no significant difference was observed in either urinary excreted Mg^{2+} or serum Mg^{2+} level for male gGT-Cre *KO* mice. The female *trpm7 KO* mice were also found to excrete same amount of Mg^{2+} as well as possess similar levels of Mg^{2+} in their blood serum compared to their control littermates (Figure 11C-11D).

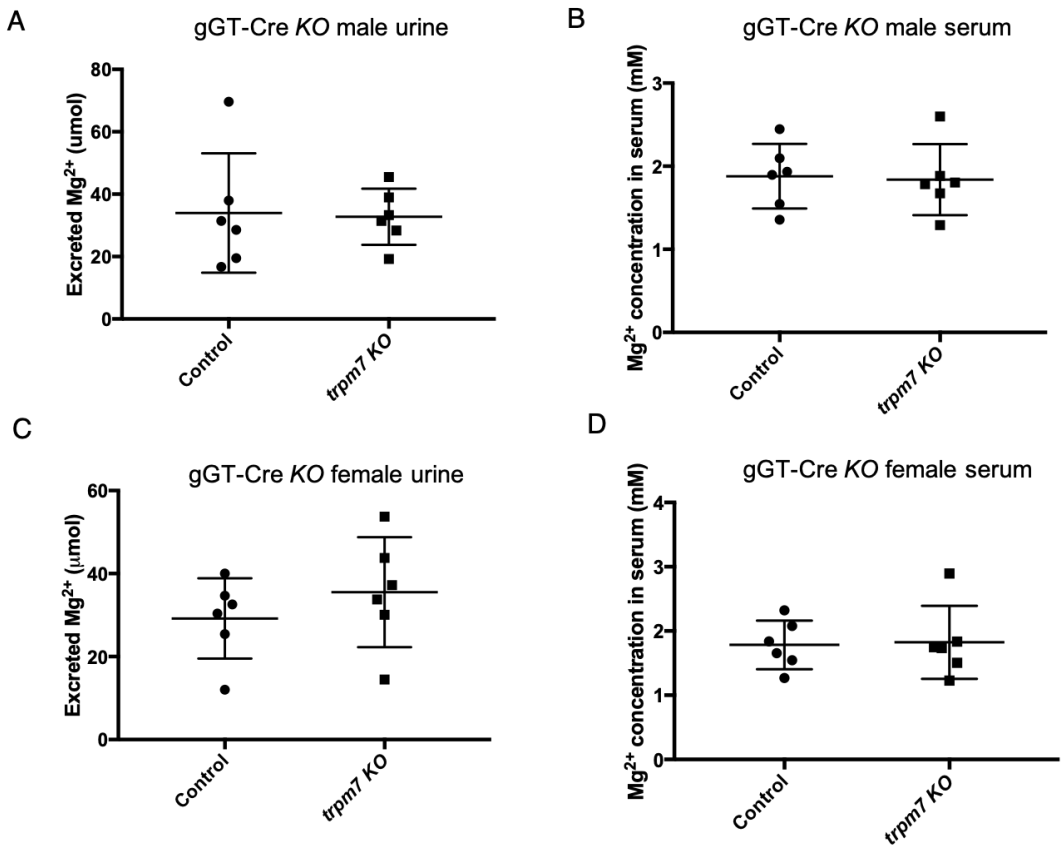

Figure 11. Disruption of *Trpm7* gene in proximal tubule by gGT-Cre recombinase did not alter the Mg^{2+} status of both male and female *trpm7 KO* mice.

(A) Comparison of the urinary excretion of Mg^{2+} in male gGT-Cre KO *trpm7* (n = 6) and control (n = 6) mice, $p = 0.895$. **(B)** Comparison of the level of Mg^{2+} in the serum of male gGT-Cre KO *trpm7* (n = 6) and control (n = 6) mice, $p = 0.868$. **(C)** Comparison of the urinary excretion of Mg^{2+} in female gGT-Cre KO *trpm7* (n = 6) and control (n = 6) mice, $p = 0.367$. **(D)** Comparison of the level of Mg^{2+} in the serum of female gGT-Cre *KO trpm7* (n = 6) and control (n = 6) mice, $p = 0.89$. Two-tailed student *t* test was used for the statistical analysis. $p < 0.05$ was considered significant. All mice used here were 30~32-week-old.

From the studies of Mg^{2+} status in both PEPCK-Cre and gGT-Cre *KO trpm7* mice, we did not observe statistically significant difference in the Mg^{2+} status of *trpm7 KO* mice and their control littermates. One possible explanation is that the Mg^{2+}-deficient phenotype generated by *trpm7 KO* in proximal tubule could be masked by compensatory Mg^{2+} reabsorption in distal nephron segments. For example, decreased Mg^{2+} reabsorption in the proximal tubule caused by loss of TRPM7 could in turn enhance Mg^{2+} reabsorption by TRPM6 in distal convoluted tubule. We took note, however, that Mg^{2+} handling in the neonatal proximal tubule was reported to be quite different than that observed in adult kidney. In immature rat, the Mg^{2+} reabsorption is predominately in the proximal tubule rather than loop of Henle [87, 88]. As such, we speculated that TRPM7 function in proximal tubules may be more easily observed in young animals. Therefore, we decided to investigate the impact of loss of TRPM7 on the Mg^{2+} status of young pups.

We collected pups at postnatal day 5-6 and took serum samples from their blood. Interestingly, young mice have higher levels of Mg^{2+} in serum than adult mice (3 *vs.* 2 mM). However, the gGT-Cre *KO trpm7* pups only showed slight lower Mg^{2+} level than their control littermates, but the difference was not statistically significant (Figure 12).

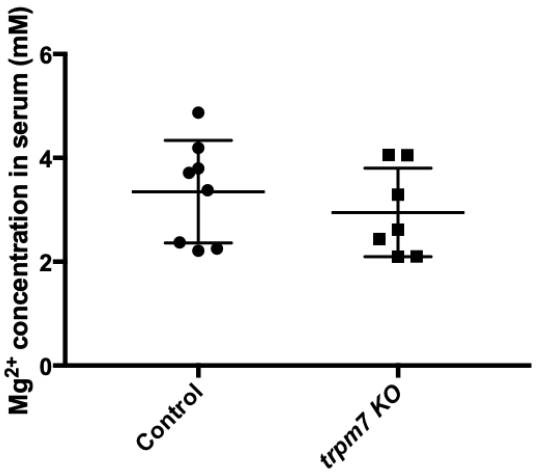

Figure 12. Assessment of the Mg^{2+} status in gGT-Cre *KO* trpm7 pups

Postnatal 5-6 days old gGT-Cre *KO trpm7* (n = 7) and control (*Trpm7*$^{flox/flox}$, n = 8) pups were sacrificed and the amount of Mg^{2+} in serum was measured. (p = 0.421).

1.3 Renal cysts in the kidneys of TRPM7-defficient mice

We did not obtain any evidence that the deletion of TRPM7 in the renal proximal tubule by Cre recombinase causes significant Mg^{2+}-deficiency in mouse. Thus, the origin of the growth deficient phenotype revealed in gGT-Cre *KO trpm7* mice remained unclear. As we have discussed in Section 1.1., about 4 out of 19 (~20%) of gGT-Cre *KO trpm7* pups were born with severe growth defect and usually died before 6 weeks of age. Among those gGT-Cre *KO trpm7* mice that survived over 6 weeks, all of them were smaller than their littermates (Figure 6).

In order to explore the pathophysiological causes of the growth defect, we dissected 15 adult female gGT-Cre *KO trpm7* animals and found that 5 of them had large cavities developed in the renal pelvis and cortex, whereas no cavities where detected in the control group (n=12). Interestingly, mice with renal cavities were much smaller than their control littermates, and their kidneys appeared to be much paler than those of control mice. The phenotype results are summarized in Figure 13. No male gGT-Cre *KO* mice were found to have renal cavities (n = 10), however, one male PEPCK-Cre *KO trpm7* mouse had similar renal cavities, suggesting that the renal cavity phenotype can also happen with males.

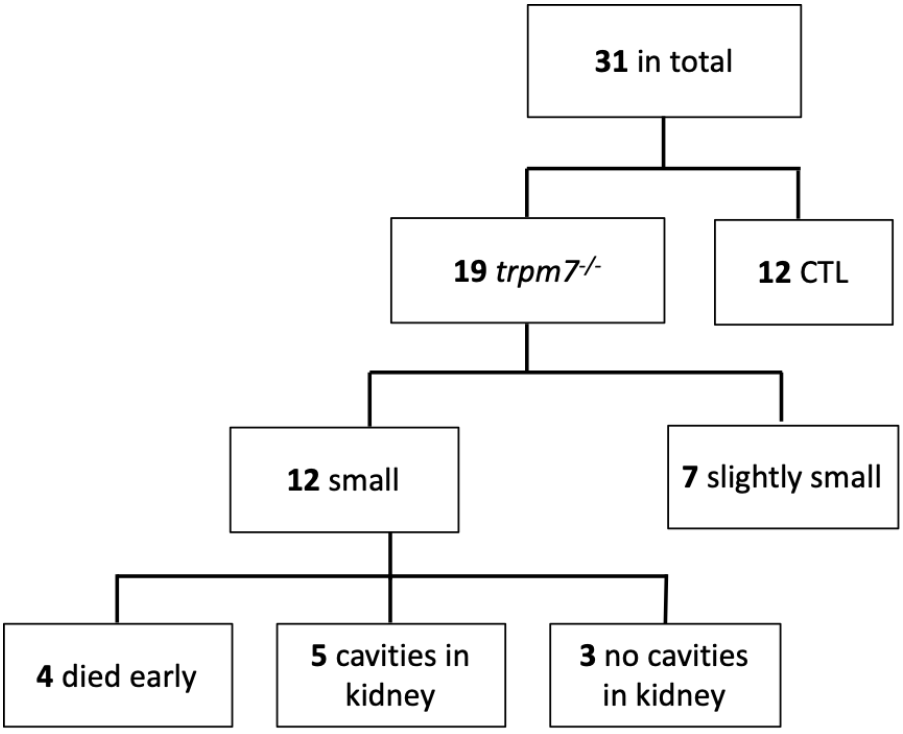

Figure 13. Summary of the phenotype of female gGT-Cre *KO trpm7* mice.

We dissected 31 female mice including 12 control Trpm7$^{fl/fl}$ mice and 19 gGT-Cre *KO trpm7* mice. Among those 19 *trpm7 KO* mice, there were 4 animals born with very small size and died before age of 6 weeks, 8 animals exhibited much smaller body size than their control littermates (about ½ of the size of their control littermates), and 7 animals were just slightly smaller than their littermates. 5 individuals in the group of very small *KO* mice were found to generate large cavities in their kidneys. All dissected mice were 30~32-week-old.

The morphological images of the 5 cavity-generated kidneys are shown in Figure 13. In gGT-Cre *KO* mice, the renal pelvis and medulla part were largely damaged. Strikingly, for some of gGT-Cre *KO* mice (# 258, #349 and #372), the renal pelvis structures were completely absent, affecting also the renal cortex. In Figure 14A, the top 4 group of kidneys were from older gGT-Cre *KO* mice at the age of 30~32 weeks. For these mice, both of the kidneys of the mutant mice had generated the large cavities. However, the two kidneys in the last group at the bottom of Figure 14A were actually from the same mouse #372 (highlighted in the red rectangle), which had one kidney with a large cavity and the second was still intact and healthy-looking. #372 was only 12 weeks old when sacrificed for kidney morphology analysis. Therefore, we speculate that the renal cavity develops later in development, starting approximately at the age of 12 weeks. In support of this hypothesis, 4 gGT-Cre *KO* mice younger than 12 weeks did not present with renal cavities (representative images are shown in Figure 14B). For example, the kidney of mouse #348 was much smaller than its control littermate, which was likely due to its much smaller body size. However, despite its unusual small kidney size, mouse #348 did not generate any cavities in its kidney.

A

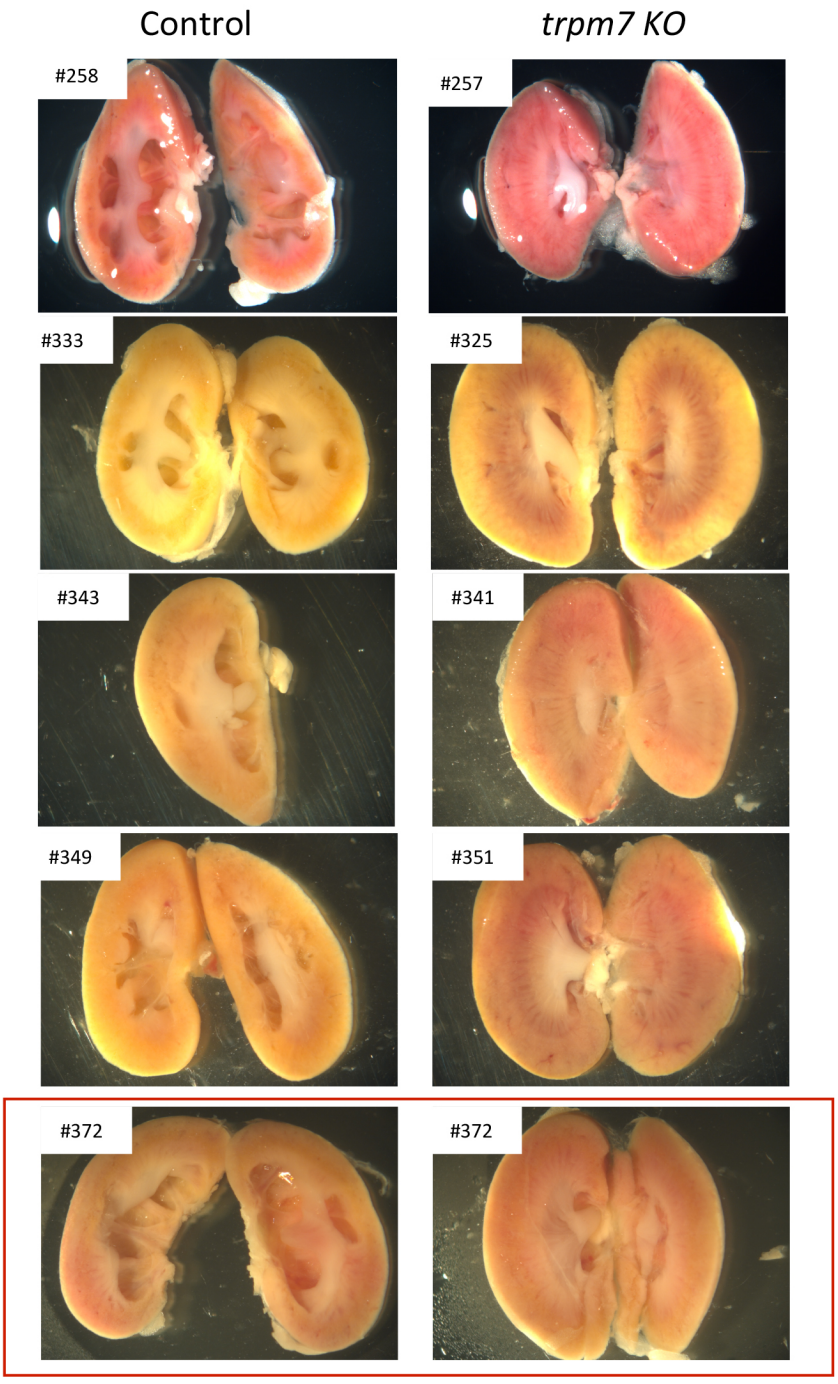

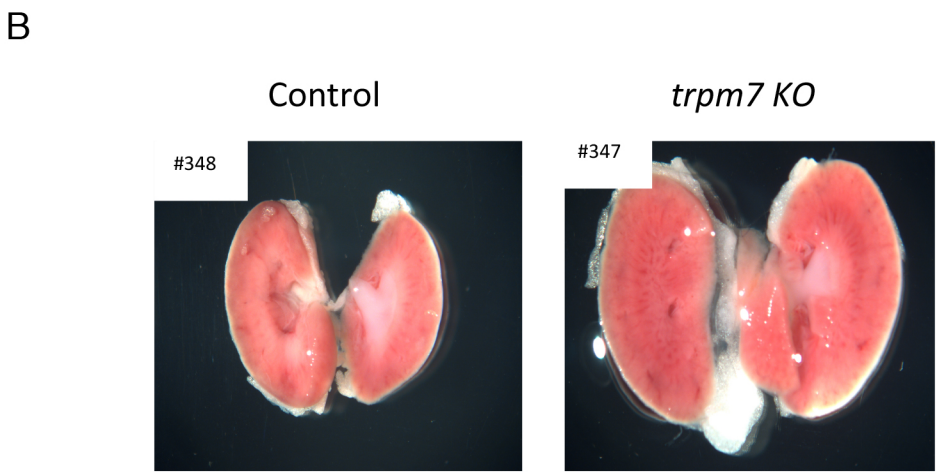

Figure 14. Morphology of cavities generated in the kidneys of female gGT-Cre *KO trpm7* mice

(A) Images showing the cavity-generated in gGT-Cre *KO trpm7* mice. All of the mice in these experiments were female 30~32-week-old gGT-Cre *KO trpm7* mice, except #372 (highlighted in the red rectangle). #372 was a 12-week-old female gGT-Cre *KO trpm7* mouse. All the older mice generated cavities in both of their kidneys, whereas in the 12-week-old younger mouse, the cavities were found only in one kidney. **(B)** Representative images from a 6-week-old gGT-Cre *KO trpm7* mouse and its control littermate. All of images are taken at the same magnification.

To gain more insight into the origin of the renal cavities, we performed histological analysis and hematoxylin and eosin staining of kidney tissues from 30-week-old and 6-week-old gGT-Cre *KO trpm7* mice. As is demonstrated in Figure 15A, the renal pelvis and the medulla structure of the older gGT-Cre *KO trpm7* mouse is largely absent. In the magnified images, the thickness of the cortical layer of the kidney was significantly reduced compared to that from the control mouse. For younger *trpm7* gGT-Cre *KO* mouse, no renal cavities were observed, however, the cortical layer of the kidney was still reduced dramatically compared to that of the control (Figure 15B). This phenotype suggests that the knockout of TRPM7 in proximal tubule might affect the cell proliferation in proximal tubule.

A

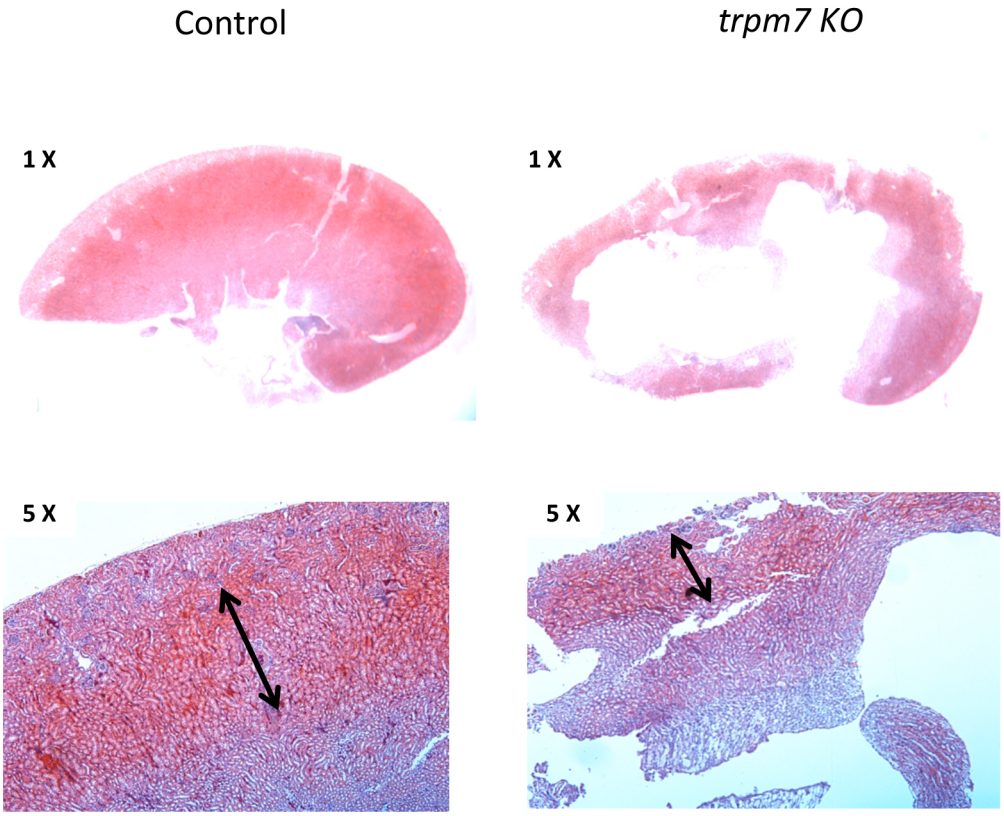

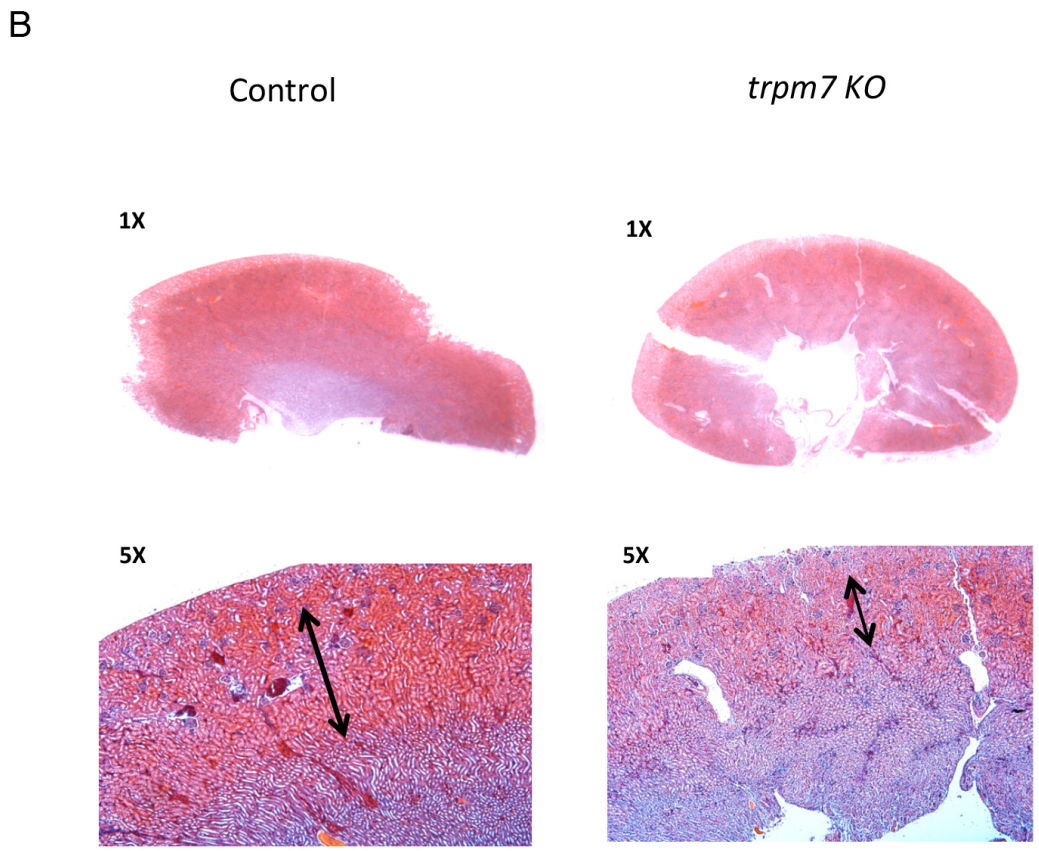

Figure 15. H&E staining of kidney sections from gGT-Cre *KO trpm7* and control mice.

(A) Representative images of the H&E staining of paraffin embedded kidney sections of a 30-week-old mouse. The top images showed that the large cavities generated in kidney severely disrupted the structure of renal pelvis and the medulla. The bottom images were magnified images showing that the thickness of the cortical layer of the kidney was significantly reduced compared to that of the control mouse. Arrows indicates the cortical layer of kidney. **(B)** Representative images of the H&E staining of paraffin embedded kidney sections of a 6-week-old mouse. In this example, no renal cavities were observed,

however, the cortical layer of the kidney was still dramatically reduced in size compared to that of the control

To determine whether the generation of renal cavities correlated with Mg^{2+}-deficiency, we specifically examined the Mg^{2+} status in those mice that had cavities generated in their kidneys. As is shown in Figure 16, the Mg^{2+} level in cavities-generated *trpm7 KO* was similar to their control littermates.

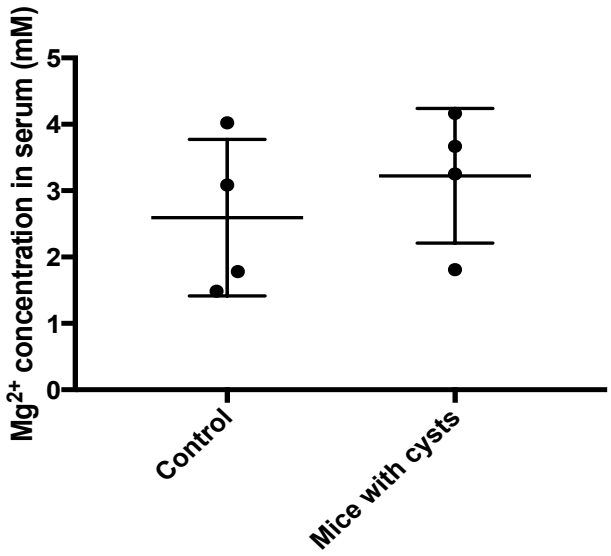

Figure 16. Assessment of the Mg^{2+} status in the mice that have renal cavities

Comparison of the Mg^{2+} level in the serum of cavity-generated gGT-Cre *trpm7 KO* mice and their *Trpm7*$^{flox/flox}$ control littermates.

SECTION II: TRPM7 and Cell-Cell Adhesion

Having observed the phenotype in the kidneys of female gGT-Cre *trpm7* KO mice, we were motivated to explore the mechanism by which the cavities in kidney were generated. TRPM7 has been reported to be involved in cellular adhesion and migration and contribute to intercellular junction formation in mouse urothelium [89]. In urothelium-specific *trpm7 KO* mice, interstitial inflammation was observed in *trpm7 KO* bladders, and the intercellular junctions were impaired in *trpm7 KO* urothelium [53]. We hypothesize that the deletion of *Trpm7* in proximal tubule disrupted the intercellular junction formation in tubular epithelial cells, resulting in kidney cavities in mouse kidney.

2.1 Impaired intercellular junctions were detected in the renal cortex of gGT-Cre *KO trpm7 mice*

To test the hypothesis that absence of the TRPM7 channel affects intercellular junction formation, we first performed a transmission electron microscopy (TEM) analysis on the renal cortex of gGT-Cre *trpm7 KO* and control ($Trpm7^{flox/flox}$) mice. We observed two type of intercellular junctions in the cortex of mouse kidney: one is a tightly sealed mature junction as was shown in Figure 17A, whereas the other type was an impaired junction that had about 20~30 nm gap between the adjacent cells (Figure 17B). We analyzed about 60 intercellular junctions in *trpm7 KO* mice and control mice and found that about 50% of the analyzed junctions in *trpm7 KO* mice were impaired junctions (Figure 17C), compared to just 20%, from control mice. This data suggests that intercellular junction formation or stability maybe disrupted in gGT-Cre *trpm7 KO* compared to control mice.

A

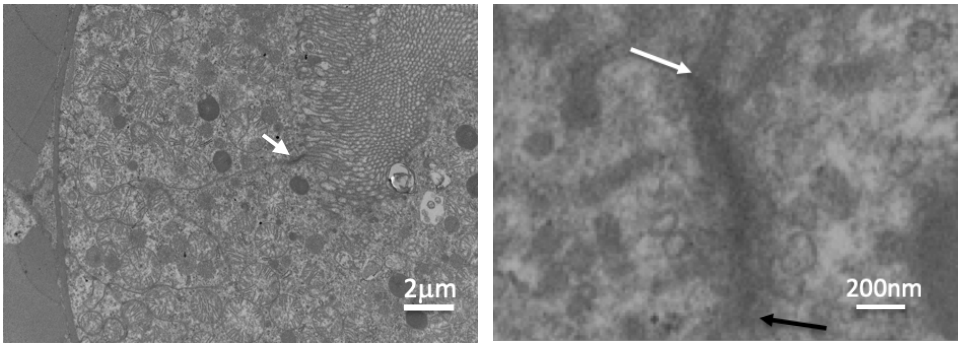

B

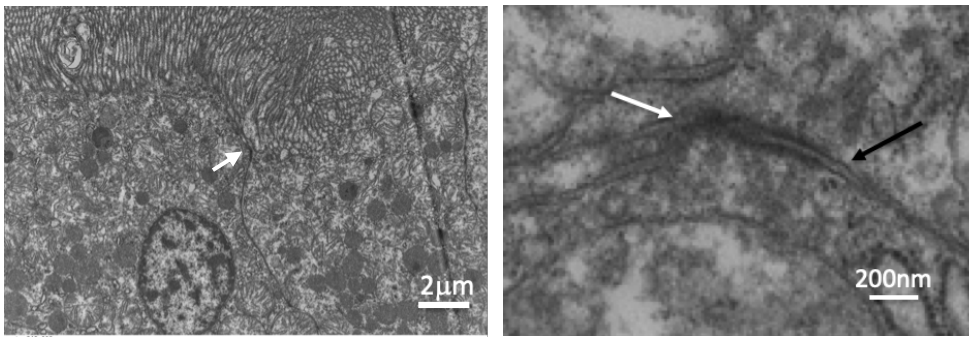

C.

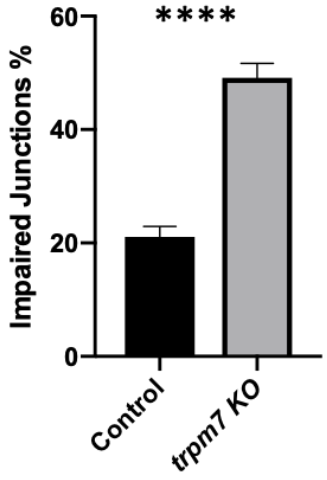

Figure 17. Electron microscopy analysis of the intercellular junctions in the cortex of mouse kidney.

(A) A representative of transmission electron microscopy of a tightly sealed junction between two adjacent epithelial cells in the cortex of mouse kidney. **(B)** A representative of transmission electron microscopy of an immature junction that has a 20-30 nm gap between two adjacent epithelial cells in the cortex of mouse kidney. In *trpm7 KO* mice, 50% of intercellular junctions are immature junctions while in the control mice, the percentage of immature junctions is only 20%. The white arrow in the left image indicates the location of the junction. The right image showed the same intercellular junction at a higher magnification. The white arrow in the right image indicates the apical side of the junction and the black arrow indicate the end point of the junction. **(C)** Comparison of the percentage of impaired intercellular junctions in *trpm7 KO* mice and the control floxed mice. 60 intercellular junctions were analyzed in each group (Mean ± S.E.M, Student *t*-test, **** $p < 0.0001$).

2.2 TRPM7 localized to the cell periphery in proximal tubule cells

To further investigate the role of TRPM7 in cell-cell adhesion in proximal tubule, we employed an established epithelial cell model. Opossum kidney (OK) cells were generated from proximal tubule of opossum, and it has been frequently used as a cell model to study the function of ion channels and transporters in kidney [68, 90, 91]. We performed immunocytochemistry of OK cells transiently expressing HA-tagged TRPM7. TRPM7 was seen weakly localized to the apical membrane of OK cells in actin patches, and prominently localized to the cell borders (lateral membranes) of the confluent cuboidal OK cells (Figure 18). This provided evidence in support our hypothesis that TRPM7 is playing a role in regulating cell-cell adhesion process in proximal tubule epithelial cells.

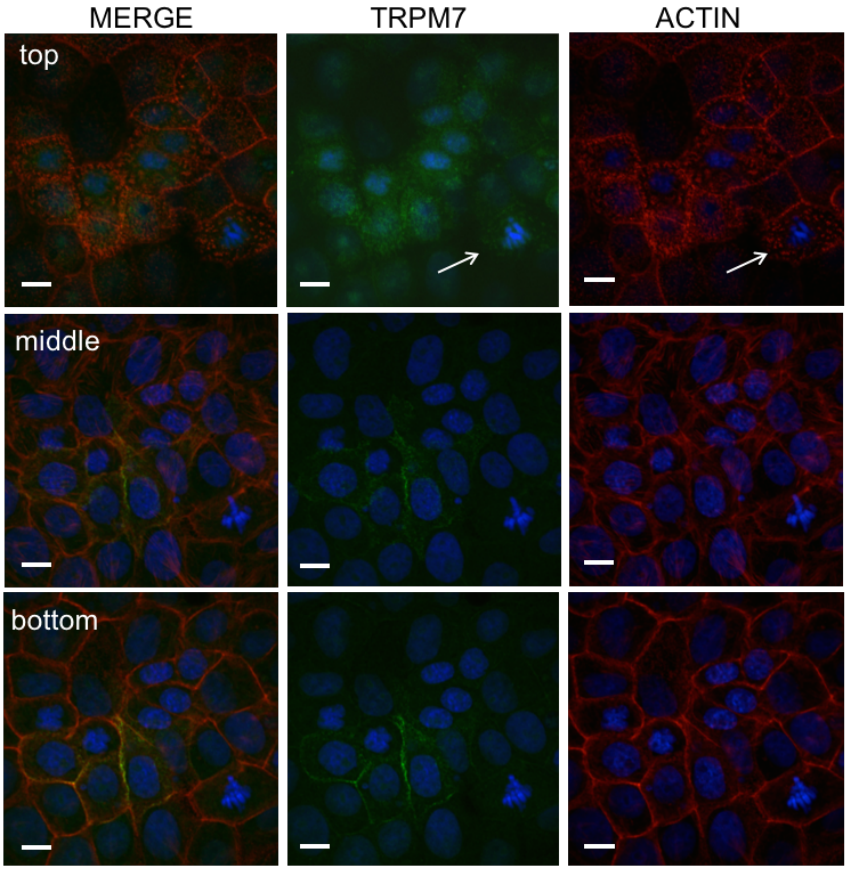

Figure 18. Representative confocal images showing cellular localization of HA-TRPM7 in OK cells.

Representative confocal Z-stack images of transiently expressed HA-TRPM7 (green) and actin (red) in opossum kidney (OK) proximal tubule epithelial cells (*Scale bar, 10 microns*). HA-TRPM7 was expressed for 24 h before subjected to immunocytochemistry. TRPM7 weakly localized to the apical membrane of OK cells in actin patches (white arrow) (top) and prominently localized to the basolateral sides of OK cells (middle and bottom).

2.3 TRPM7 interacted and co-localized with cell adhesion junction proteins

To learn more about how TRPM7 may be affecting cell-cell adhesion, we performed mass spectrometry analysis of HA-tagged TRPM7 immunopurified from OK cells. Included among the potential interacting proteins we identified were two cell adhesion proteins, plakoglobin and desmoplakin. Plakoglobin is also known as junction plakoglobin or γ-catenin and is a cytoplasmic component of adherens junctions and desmosomes. In adherens junctions, plakoglobin binds to E-cadherin's cytoplasmic domains to form the cadherin-catenin complex (CCC), which plays a fundamental role in mammalian development and tissue morphogenesis [92, 93]. In desmosomes, plakoglobin forms a dense plaque together with desmoplakin to link two types of desmosomal cadherins, desmoglein (Dsg) and desmocollins (Dsc) to intermediate filaments to provide strength to cells that experience intense mechanical stress [94-96]. Figure 19A shows the molecular organization of adherens junctions and desmosomes and the localization of plakoglobin and desmoplakin in these cellular structures.

To learn more about TRPM7's function in cell-cell adhesion we investigated TRPM7's ability to co-localize with plakoglobin and desmoplakin, a marker of desmosomes. We performed immunocytochemistry on OK cells co-transfected with TRPM7 and Myc-tagged plakoglobin or GFP-tagged desmoplakin. Comparing the immunostaining results in Figure 19B, we conclude that TRPM7 exhibited better co-localization with plakoglobin than desmoplakin, indicating that TRPM7 may be affecting cell-cell adhesion function more in adherens junctions rather than in desmosomes.

A

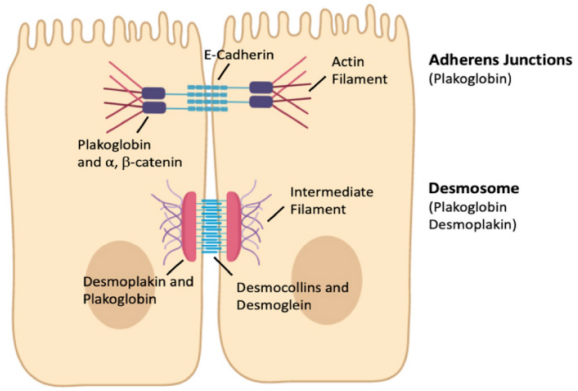

B

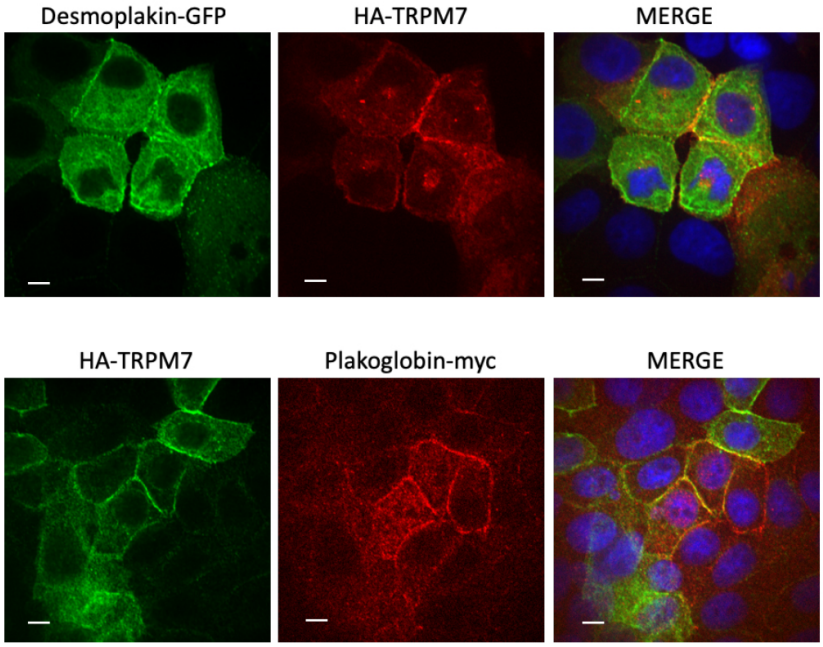

Figure 19. TRPM7 co-localizes with plakoglobin (γ-catenin) to cell adhesion junctions

(A) A brief diagram of the formation and position of adherens junction and desmosome in epithelial cells. In the adherens junctions, the cytoplasmic side of E-cadherins are linked to actin filaments through plakoglobin and other catenins (α-catenin and β-catenin). While in the desmosome complex, the desmosomal cadherins, desmoglein (Dsg) and desmocollins

(Dsc) link to intermediate filaments through plakoglobin and desmoplakin. **(B)** Confocal images of OK cells co-transfected with TRPM7 and desmoplakin (top) or plakoglobin (bottom) (*Scale bar 10 micron*). TRPM7 is observed to better co-localize with plakoglobin than desmoplakin.

Having found that TRPM7 co-localizes better with plakoglobin than desmoplakin, a marker of desmosomes, we next sought to determine whether TRPM7 is a bona fide component of adherens junctions. To clarify the localization TRPM7 in OK cells, we employed E-cadherin as an adherens junction marker for immunocytochemistry analysis. HA-TRPM7 was transiently transfected into OK cells. Cells were fixed and stained with anti-HA antibody to recognize TRPM7 (Green) and an antibody against E-cadherin to recognize the endogenous protein (red). Z-stack images were taken by confocal microscopy (Figure 20). We analyzed a cross-section of the cell border between two adjacent cells and found that TRPM7 highly co-localized with E-cadherin in adherens junctions in OK cells.

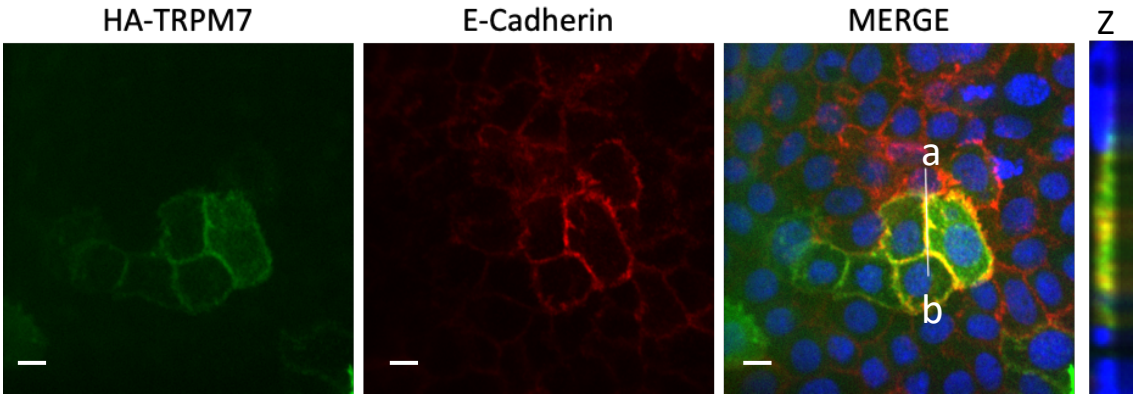

Figure 20. TRPM7's colocalization with E-Cadherin in adherens junctions in OK cells.

Representative confocal Z-stack images indicating the colocalization of transiently expressed HA-TRPM7 (green) and endogenous E-cadherin (red) in opossum kidney (OK) proximal tubule epithelial cells (*Scale bar, 10 microns*). A cross section through the border of two neighboring cells along the line, from a to b in the merged image showed that HA-TRPM7 colocalized with endogenous E-cadherin to the same depth of lateral side of OK cells. The Z plane runs from bottom (left) to top (right).

2.4 TRPM7's channel function affects cell-cell adhesion junctions in OK cells

Our results thus far suggest a role for TRPM7 in cell adhesion. The next question to asked was whether TRPM7's function was involved in regulating cell adhesion process. We first tested whether TRPM7's channel activity would have an effect on cell adhesion. TRPM7 channel inhibitor (NS8593) and channel opener (Naltriben mesylate) were applied to OK cells and the alteration of cell adhesion process in responding to the modulation of TRPM7's channel function was evaluated using E-cadherin, a marker of adherens junctions. As was shown in Figure 21, blocking TRPM7's channel activity reduced E-cadherin's expression level and its localization to the adherens junctions, indicating that the level of intercellular junctions formation was diminished. The treatment with channel opener increased the E-cadherin level, however, it also impaired the localization of E-cadherin in the adherens junctions. A large amount of E-cadherins was found localized in the cytosol.

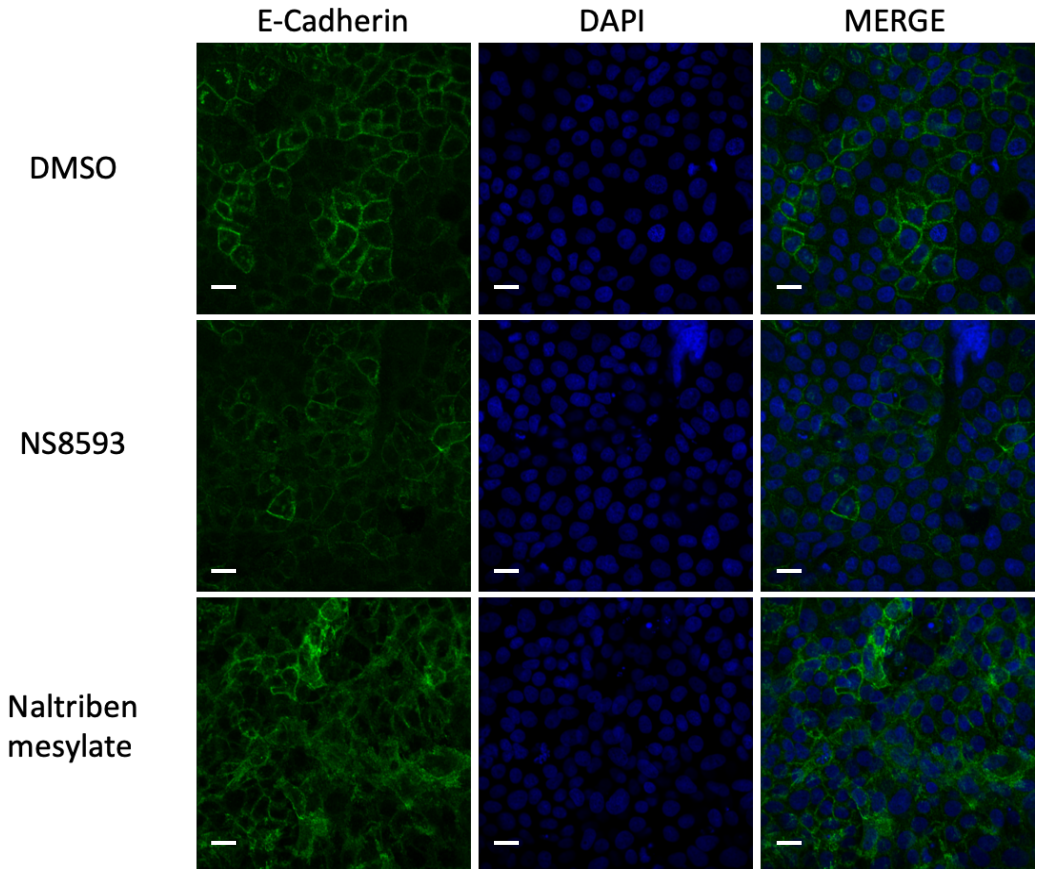

Figure 21. The effect of TRPM7's channel activity on E-Cadherin localization.

Confocal images of adherens junction protein, E-cadherin's localization in OK cells in responding to the treatment of TRPM7 channel inhibitor (NS8593) and channel opener (Naltriben mesylate). (*Scale bar 10 micron*). Blocking TRPM7's channel activity reduced E-cadherin's expression level and its localization to the cell membrane. The treatment with channel opener increased the E-cadherin level, however, it also impaired the localization of E-cadherin to adherens junctions.

SECTION III: NHERF Proteins and TRPM7's Regulation in Epithelial Cells

In the previous chapters, we investigated the role of TRPM7 in mouse proximal tubule. Our results indicate that TRPM7 appears to play only a minimal role in regulating Mg^{2+} transport in the proximal tubule. Instead, we found evidence that TRPM7 is involved in the cell-cell adhesion process. In addition to finding TRPM7 localized to adherens junctions we also observed TRPM7 localized to the apical membrane of proximal tubule cells, where it is found in actin-rich patches (Figure 17). In this section, we investigate the hypothesis that TRPM7's localization to proximal tubule epithelial cells is regulated by TRPM7's PDZ-binding motif and members of the PDZ-domain scaffolding protein family, NHERF.

3.1 Interaction between TRPM7 and NHERF proteins requires TRPM7's PDZ-binding motif

We performed a yeast two-hybrid screen using the COOH-terminus of TRPM7 and identified NHERF3 and NHERF4 as potential interacting proteins. To confirm the *in vivo* interaction between TRPM7 and NHERF3, FLAG-tagged NHERF3 was transiently expressed in tetracycline-inducible HA-TRPM7 cells and subjected to immunoprecipitation (Figure 22A). The result showed that FLAG-NHERF3 readily co-immunoprecipitated with HA-TRPM7, indicating a *bona fide* interaction between these two proteins.

An *in vitro* GST pull-down purification assay also verified NHERF3 as a *bona fide* TRPM7 binding protein as well as demonstrated the capacity of other members of the NHERF family to interact with the channel (Figure 22A and B). We created two GST fusion proteins, one was called GST-C47, which had the last 47 amino acids of TRPM7

fused to GST, the other one was called GST-C47ΔPDZ with the last 6 amino acid of GST-C47 deleted from its carboxyl terminus. The last 6 amino acid was known to usually compose the PDZ-binding motif of ion channels and transporters [64]. Using these two GST fusion proteins, we conducted the pull-down assay against four FLAG-tagged NHERF family members in cell lysates and found that all of the NHERF proteins were readily pulled down by GST-C47 but not GST-C47ΔPDZ. The fact that TRPM7 can bind to multiple NHERF proteins is not surprising as the individual NHERF genes are thought to have evolved through gene duplication events, with high sequence similarity among individual PDZ domains. In addition, the pull-down assay confirmed the functionality of TRPM7's PDZ-binding motif, demonstrating that the last six amino acids of TRPM7 are required to mediate the protein-protein interaction.

Studies have shown that the 4 PDZ domains in NHERF3 can bind to different target [97]. For example, NHERF3's 1st PDZ domain can bind to PLC-β, its 2nd domain can bind to parathyroid hormone receptor (PTH1R) as well as other G protein coupled receptors, and the 3th and 4th PDZ domain of NHERF3 can heterodimerize with NHERF1 to augment NHERF1 function *in vivo* [97, 98]. We investigated which of NHERF3's PDZ domain(s) is responsible for the interaction between TRPM7 and NHERF3. Our experiments revealed that TRPM7's COOH terminus binds to the 2nd PDZ domain of NHERF3 (Figure 22C).

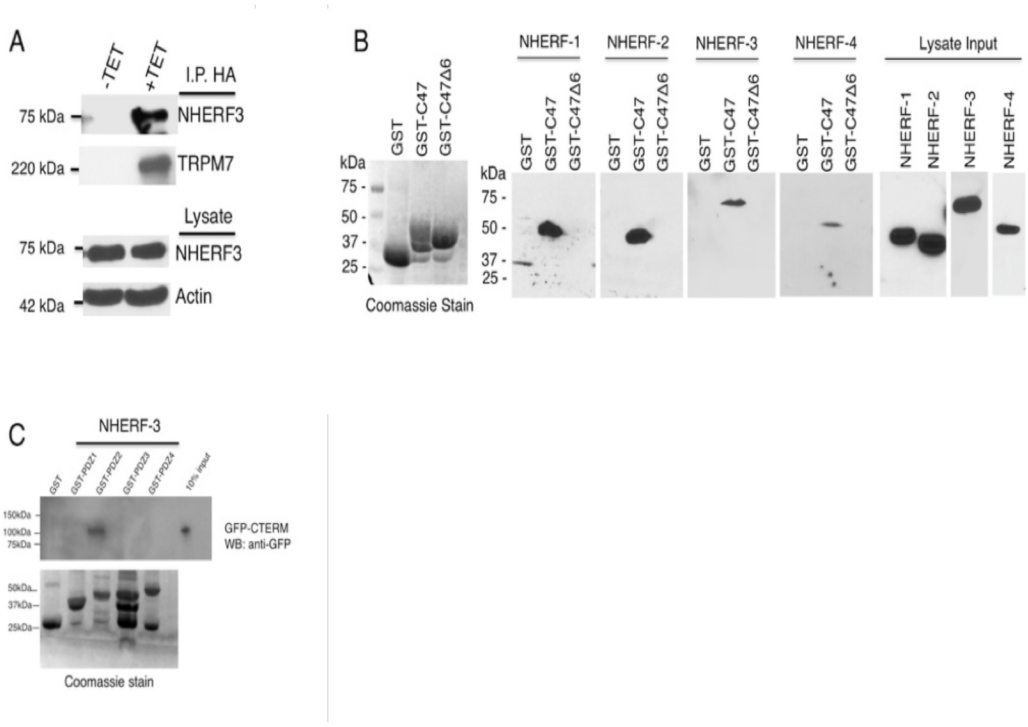

Figure 22. Interaction between TRPM7 and NHERF proteins requires TRPM7's PDZ-binding motif.

(A) 293-TRPM7 cells, which express HA-tagged TRPM7 in response to tetracycline, were transiently transfected with FLAG-tagged NHERF. NHERF3 co-immunoprecipitated with HA-TRPM7. **(B)** For our GST-pulldown assay we used purified GST, GST-C47, which contains the last 47 amino acids of TRPM7, and GST-C47Δ6 (GST-C47ΔPDZ), which lacks the last six amino acids of GST-C47. GST, GST-C47 and GST-C47Δ6 bound to glutathione agarose beads were incubated with cell lysate derived from HEK-293T cells expressing FLAG-tagged NHERF proteins NHERF1, NHERF2, NHERF3 and NHERF4 (Left). Coomassie staining demonstrated that similar amounts of GST-C47, GST-C47ΔPDZ and GST were used in the assay (Right). Bindings of all of the 4 NHERF

proteins were detected by immunoblotting with FLAG antibody. (C) We employed a GST pull-down assay to map which PDZ domains in NHERF3 bind TRPM7 using individual GST-PDZ proteins against TRPM7 COOH-term fragment GFP-CTERM (a.a. 1288-1862 of TRPM7) and found that NHERF3's 2nd PDZ domain binds to TRPM7.

3.2 The functional significance of TRPM7's PDZ-binding motif

Next, we asked what the functional significance of this PDZ-binding motif of TRPM7 is. To answer this question, we constructed a mutant version of HA-TRPM7 by deleting the PDZ-motif from the carboxyl terminus of HA-TRPM7 (HA-TRPM7ΔPDZ). We generated tetracycline inducible HA-TRPM7ΔPDZ stable cell line to study the impact of TRPM7's PDZ-binding motif on TRPM7 protein expression and channel function.

We first investigated whether the deletion of PDZ-motif would affect the expression of TRPM7. HA-TRPM7 WT and HA-TRPM7ΔPDZ were heterologously expressed in 293T cells. After 24 hours, cells were lysed, and the cell lysates subjected to SDS-PAGE and Western blot analysis. Our results showed that HA-TRPM7ΔPDZ had the same expression level as HA-TRPM7, indicating PDZ-binding motif does not have effect on protein expression (Figure 23A).

We next investigated whether TRPM7's PDZ-binding motif would affect electrophysiological function of TRPM7. Following 24 hours of tetracycline induction, HA-TRPM7ΔPDZ and wildtype control cells were plated on Poly-L-lysine coated tissue culture dishes and subjected to patch clamp analysis to measure their whole-cell currents. It was found that HA-TRPM7ΔPDZ cells produced robust TRPM7-like current, which indicate that the deletion of PDZ-binding motif did not significantly compromise TRPM7's channel activity (Figure 23B).

We next investigated whether TRPM7's PDZ-binding motif influenced the cellular localization of TRPM7 in OK cells. TRPM7ΔPDZ and TRPM7 WT were transiently expressed in OK cells for various times up to 96 hours. After 24 hours of expression, about 63% of TRPM7 WT protein localized to the basolateral side and at the periphery of OK cells (Figure 23A and 23B), compared to 60% for TRPM7ΔPDZ, suggesting that the PDZ-

binding motif had no significant effect on cellular trafficking of TRPM7 to plasma membrane. After 24 h, the percentage of cells showing border localization of TRPM7 increased until reaching its maximum (~69.8%) at 48 h. A relatively high percentage of cells have TRPM7 WT at the cell border up to 72 h, after which time localization of TRPM7 at the periphery begins to decrease. On the other hand, TRPM7ΔPDZ was found at high levels at the cell border for only 48h. and then decreased by 72 h. These results suggest that TRPM7's PDZ-binding motif stabilizes the channel's localization to the cell border. One possibility to explain these results is that when TRPM7 lacks the PDZ-binding motif the channel's ability to interacting with a PDZ-containing scaffolding protein is disrupted, making the channel more vulnerable to internalization and/or protein turnover.

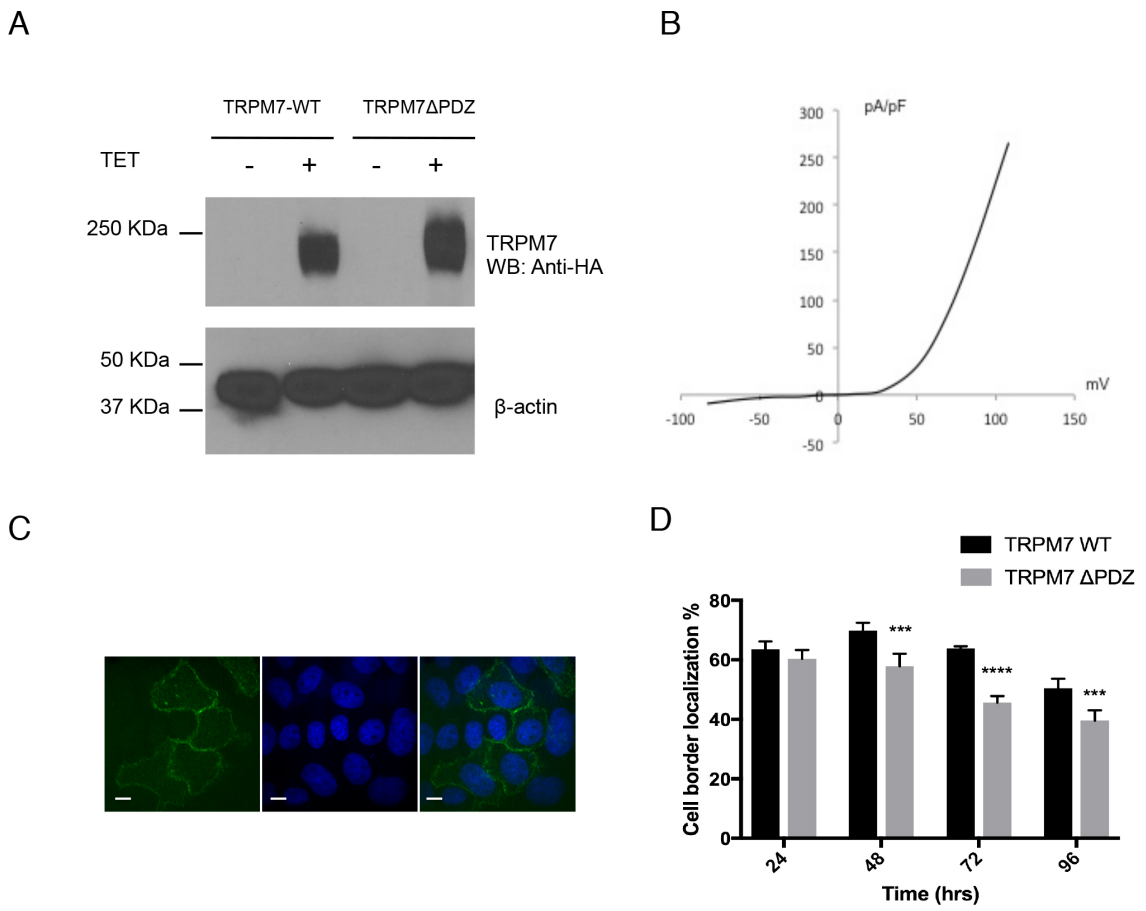

Figure 23. The functional significance of PDZ-binding motif

(A) The deletion of PDZ-binding motif did not alter the expression level of TRPM7ΔPDZ in HEK-293 cells. After 24 h of tetracycline induction, HA-TRPM7 WT and HA-TRPM7ΔPDZexpressing cells were lysed. The expression of TRPM7 and TRPM7ΔPDZ in cell lysates were assessed by SDS-PAGE and Western blotting using anti-HA antibody. **(B)** Whole cell recording of TRPM7ΔPDZ. Similar to TRPM7-WT, TRPM7-ΔPDZ current shows a large outwardly rectifying conductance at positive potential and a small inward conductance at negative potential. (C) Representative confocal image of TRPM7 localizing to the basolateral side and at the periphery of OK cells. HA-TRPM7 was transiently

transfected in OK cells. Cells were fixed at different time points and stained with anti-HA (Rabbit, primary) and Alexa Fluor™ 488 (Goat anti Rabbit, secondary) antibodies. (D) Quantitative analysis of the percentage of the cellular localization of transiently transfected HA-TRPM7 and HA-TRPM7ΔPDZin OK cells for different length of time. 600-700 cells from six independent experiments were examined for each group (Mean ± S.E.M, Student *t*-test, *** $p < 0.0005$, **** $p < 0.0001$).

3.3 NHERF proteins interact with TRPM7 but do not regulate the channel

NHERF proteins have been reported to enhance the stability of their binding partners on plasma membrane by tethering them to the cytoskeleton [68, 91]. We have identified that TRPM7 interacts with NHERF proteins through TRPM7's PDZ-binding motif and that the channel's PDZ-binding motif affects TRPM7's concentration on plasma membrane. To determine whether it is NHERF proteins affect TRPM7 localization to the periphery of OK cells, we performed immunocytochemical assays on OK cells co-transfected by HA-tagged TRPM7 with FLAG-tagged NHERF proteins. After 48 hours of expression, cells were fixed and stained with anti-HA and anti-FLAG antibodies. By confocal microscopy analysis, we observed that that NHERF proteins tended to localize to the cytosol and microvilli at the apical surface of OK cells, while TRPM7 primarily localized to the basolateral side of the cells (Figure 24A). This result demonstrates that even though TRPM7 can interact with NHERF proteins biochemically *in vitro*, NHERF proteins are not able to recruit the channel to microvilli *in vivo*.

We next analyzed whether the co-expression of NHERFs would indirectly affect the cellular localization of TRPM7. If it was NHERFs that were responsible to stabilize TRPM7 to the plasma membrane, we would expect to observe a significantly higher percentage of WT TRPM7 localizing to the cell border with the presence of NHERFs than that of TRPM7ΔPDZ which was lack of the PDZ-binding motif. However, as was shown in Figure 24B, co-expression of NHERF proteins did not enhance the cell border localization of WT TRPM7, which further supports our conclusion that TRPM7 is not regulated through NHERF proteins.

A

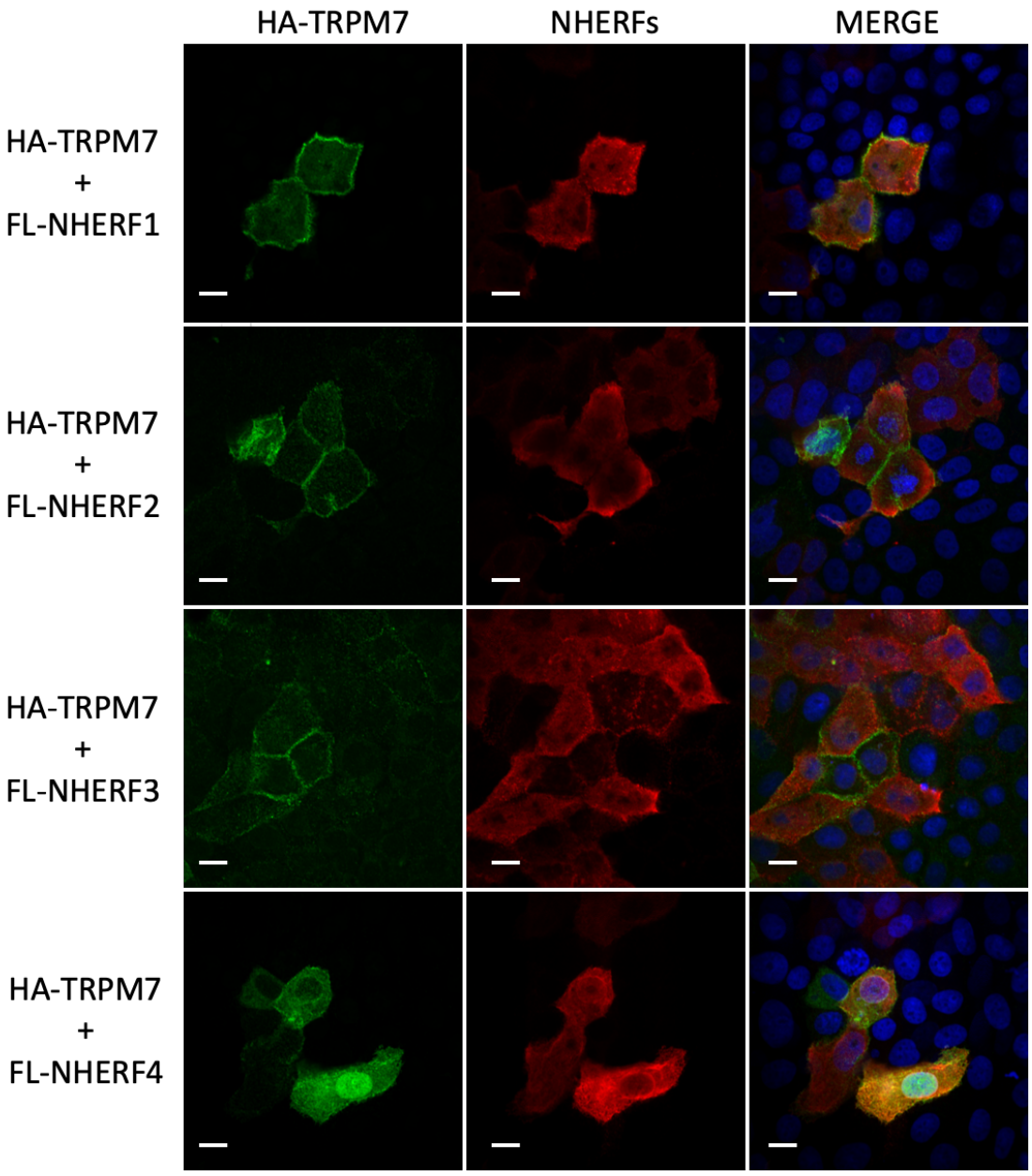
HA-TRPM7
NHERFs
MERGE
HA-TRPM7 + FL-NHERF1
HA-TRPM7 + FL-NHERF2
HA-TRPM7 + FL-NHERF3
HA-TRPM7 + FL-NHERF4

B

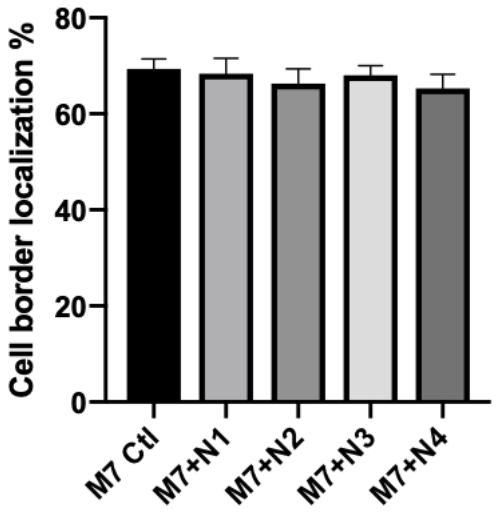

Figure 24. NHERF proteins and the cellular localization of TRPM7 and TRPM7ΔPDZ

(A) Representative confocal images showing localization of transiently expressed HA-TRPM7 (green) and FLAG-NHERFs (red) in OK cells. (*Scale bar, 10 microns*). TRPM7 prominently localized to cell border and weakly localized to the apical membrane of OK cells, while NHERF proteins tended to localize to the cytosol and the microvilli (pointed by white arrow) at the apical surface of OK cells. **(B).** Statistical analysis of TRPM7's cell peripheral localization with/without the presence of NHERF proteins. 600-700 cells from six independent experiments were analyzed for each group (Mean ± S.E.M, Student t-test, * $p < 0.05$ was considered significantly different).

3.4 Stimulation of PKC pathway affects TRPM7's cellular localization

Previous studies have shown that TRPM7 is regulated by pathways coupled to phospholipase C [9]. The localization of proteins to adherens junctions in particular is regulated by protein kinase C (PKC) [99]. As a first step towards determining whether the cellular localization of TRPM7 in proximal tubules cells is modulated by PKC, we applied an activator and an inhibitor of PKC to OK cells transiently transfected with TRPM7. OK cells were transfected with TRPM7 using Lipofectmine3000 reagent from Invitrogen. After 48 h, the transfected cells were treated either by 2 μM of PKC inhibitor chelerytrine for 6 h or by 20 nM of PKC activator Phorbol-12-myristate 13-acetate (PMA) for 2 h. Cells were fixed after treatment and subjected to immunocytochemical analysis to evaluate the percentage of the cells that were localized to the cell border. Representative images of TRPM7's localization in OK cells after stimulated by PMA and chelerytrine were shown in Figure 25A, adding PMA promoted TRPM7 to localize to the cell border while adding chelerytrine reduced the ability of TRPM7 to localize to the cell border. The quantification of the percentage of TRPM7 detected on cell border suggested that the effect of PKC modulators on TRPM7's cellular localization was statistically significant (Figure 25B).

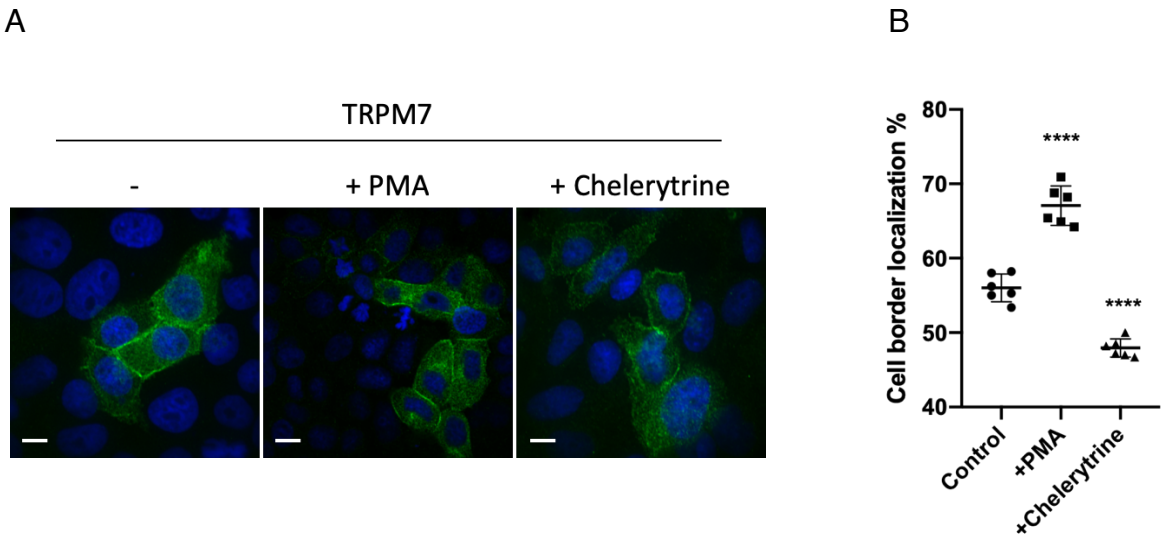

Figure 25. The effect of PKC pathway on TRPM7's localization in OK cells

(A) Representative Confocal images of TRPM7 localization in OK cells in responding to the treatment of the activator (PMA) and inhibitor (Chelerytrine) of PKC pathway (*Scale bar 10 micron*). **(B)** Statistical analysis of TRPM7's cell peripheral localization in responding to the stimulations on PKC pathway. 600-700 cells from six independent experiments were analyzed for each group (Mean ± S.E.M, Student t-test, **** $P<0.0001$).

DISCUSSION AND FUTURE DIRECTIONS

The aim of this study was to determine the role of TRPM7 ion channel in renal proximal tubule. Since TRPM7 has frequently been reported to be involved in the regulation of magnesium homeostasis, our first aim of this study was to determine whether TRPM7 was the responsible modulator for regulating magnesium homeostasis in the proximal tubule. We generated two strains of proximal tubule-specific *trpm7 KO* mice using two Cre recombinases, PEPCK-Cre and gGT-Cre. The *trpm7 KO* mice produced by both Cre recombinase were viable. PEPCK-Cre *KO trpm7* mice did not show conspicuous abnormalities in appearance and behavior except that the female *trpm7 KO* mice had lower body weight than the control $Trpm7^{flox/flox}$ mice. gGT-Cre *KO trpm7* mice showed more severe growth retardation phenotype than PEPCK-Cre *KO* mice, which may be because gGT-Cre had better penetration efficiency than PEPCK-Cre recombinase. 20% of the female gGT-Cre *KO trpm7* mice were born with a severe growth retardation phenotype and died before the age of six weeks (Figure 6). The remainder of the gGT-Cre *KO trpm7* mice were all found to have lighter body weight than the control $Trpm7^{flox/flox}$ group (Figure 7).

We speculate that the growth defect of gGT-Cre *KO trpm7* mice might be due to Mg^{2+}-deficiency, which could be caused by the loss of function of TRPM7 in proximal tubule. However, from our assessments of the Mg^{2+} status in all adult *KO* and control mice, we did not observe that knockout of *Trpm7* in mouse proximal tubule caused Mg^{2+}-deficiency in mouse. Even under the Mg^{2+} deprivation conditions, the gGT-Cre *KO trpm7* mice were still able to keep Mg^{2+} level in blood as balanced as the control mice (Figure 8-11). One straightforward explanation for these results is that TRPM7 does not mediate

Mg^{2+} reabsorption in proximal tubule. Alternatively, other Mg^{2+} transporters expressed in proximal tubule may compensate for the absence of TRPM7 when the channel is knocked-out from the proximal tubule. Another possibility is that knockout of *Trpm7* did cause insufficient Mg^{2+} reabsorption in proximal tubule, however, because proximal tubule is one of the early segments of the nephron, increased Mg^{2+} reabsorption occurred at more distal segments (thick ascending limb of the loop of Henle or distal convoluted tubule) of the nephron could compensate for the decreased absorption of Mg^{2+} in the proximal tubule. To eliminate the interference of other segments of the nephron, we took advantage of the different Mg^{2+} handling pattern in young pups, knowing that the Mg^{2+} reabsorption in immature rat predominately occurs in the proximal tubule rather than the loop of Henle. We investigated the Mg^{2+} status in P5~P6 pups and found that even at an early growth stage, the gGT-Cre *KO trpm7* mice did not show evidence of an Mg^{2+}-deficient phenotype.

Therefore, we conclude that TRPM7 does not play a major role in proximal tubule in the regulation of whole-body magnesium homeostasis. Indeed, there may be other Mg^{2+} transporters in proximal tubule that operate to regulate whole-body magnesium homeostasis. A recent study published by Mittermeier et al also investigated TRPM7's role in magnesium homeostasis using kidney- or intestine conditional knockout mice. The results revealed that deletion of *Trpm7* by *Ksp1.3-Cre* in the collecting duct, distal convoluted tubule and thick ascending limb of the nephron has no effect on Mg^{2+} homeostasis, whereas the disruption of *Trpm7* in intestine caused profound Mg^{2+} deficiency in mice [60]. Thus, both our data and the recent findings by Mittermeier et al point to another role for TRPM7 in kidney than regulating Mg^{2+} homeostasis.

Even though the knockout of *Trpm7* in proximal tubule did not cause the Mg^{2+}-deficient phenotype in gGT-Cre *KO trpm7* mice, we did find some abnormality in the

kidney anatomy of the female gGT-Cre *KO trpm7* mice. One third of female *KO* mice were found to have large cavities generated in their kidney, which severely disrupted the structure of renal pelvis and cortex of kidney (Figures 13-14). The histological analysis of *trpm7 KO* mice at younger age suggested that the cavities did not appear until the mice were past 12 weeks old (Figure 14B). The histological analysis of the kidney from old gGT-Cre *KO trpm7* mice revealed that in addition to those large cavities, the mutant mice also had thinner cortical layer comparing to those control Trpm7$^{flox/flox}$ mice, which could be due to the loss of function of *Trpm7* in proximal tubule given that TRPM7 is required for cell proliferation (Figure 14) [30, 47]. These results are reminiscent of a similar phenotype observed by Jin et al for their investigation of TRPM7's role in mouse kidney development. The metanephric mesenchyme-specific deletion of *Trpm7* using Pax3-Cre recombinase generated cysts in the proximal tubules of *KO* mice, and showed reduced glomeruli number and dilated proximal tubule [50]. Even though the cysts generated in their *KO* mice emerged at a much earlier stage, P4, we speculated that these two cavity/cyst-generated phenotypes may share a similar mechanism of origin.

For instance, Watanabe et al reported that *Trpm7* contributed to the intercellular junction formation in the urothelium, finding that deletion of *Trpm7* in urothelium impaired the intercellular junction in mouse urothelial cells [53]. To explore the possibility that TRPM7 also has a similar role in cell-cell adhesion process in proximal tubule, we performed a transmission electron microscopy analysis on the cortex of gGT-Cre *KO trpm7* mice. The results showed that the gGT-Cre *KO trpm7* mice had more impaired adhesion junctions comparing to their control littermates, which implicated that TRPM7 may be also involved in cell-cell adhesion in proximal tubule (Figure 17).

Our understanding of the relationship between TRPM7 and cell adhesion as well as cell-cell adhesion remains ambiguous. A study in neuroblastoma cell line demonstrated that overexpression of TRPM7 at a lower level would increase focal adhesion formation and cellular spreading. In addition, this study also revealed that TRPM7 regulated actomyosin relaxation and myosin filament stability to alter the cellular cytoskeleton by phosphorylating myosin II [15]. TRPM7 was also reported to be required for breast tumor cell metastasis. Mechanistic investigations revealed that TRPM7 played a role in regulating myosin II-based cellular tension, thereby modifying focal adhesion, cell-cell adhesion and polarized cell movement [100]. However, it has also been reported that overexpression of TRPM7 in HEK239 cells led to cellular swelling and loss of adhesion [4]. Su et al revealed that overexpression of TRPM7 in HEK293 cells caused cell-rounding with a concomitant loss of cell adhesion through m-calpain (a Ca^{2+} dependent protease) by mediating the local influx into peripheral adhesion complex [24]. These conflicting results may reflect experimental differences in cell types and TRPM7 overexpression level. Further investigations are definitely required to resolve how TRPM7 may influence cell adhesion and even cytoskeletal remodeling. We expect that the results from our study of the role of TRPM7's proximal tubule epithelial cells will shed more light on this area of study.

We adopted the proximal tubule epithelial cell line OK cells as a cellular model to examine the role of TRPM7 in proximal tubule cells. OK cells are polarized epithelial cells frequently used to study the localization of ion channels and transporters that are natively expressed in the kidney proximal tubule [101]. The immunocytochemistry analysis of the TRPM7's localization in OK cells found that when heterologously expressed, TRPM7 is more readily localized to the basolateral membrane in the OK cells and to a lesser extent to the apical membrane (Figure 18). In polarized kidney epithelial cells, the apical

membrane is where ion exchange occurs between the cells and the tubular fluid. The localization preference of TRPM7 at the basolateral instead of apical side pointed to additional evidence to support that the channel may be involved in cell-cell adhesion in proximal tubule.

Another piece of evidence in support of TRPM7's role in cell-cell adhesion was the identification of two adhesion junction proteins, plakoglobin and desmoplakin by mass-spectrometric analysis, as potential TRPM7-interacting proteins. The results of immunocytochemistry analysis suggested that TRPM7 co-localized with plakoglobin rather than desmoplakin in OK cells, indicating that TRPM7 is associated with adherens junctions but not desmosomes (Figure 19). The reason why desmoplakin was also detected by mass-spectrometric analysis could be that it interacts with plakoglobin to form a complex in the immunoprecipitation cell lysate and had been pulled down together with plakoglobin and TRPM7. To verify the accurate localization of TRPM7 to cell adhesion junctions, we employed an adherens junction marker, E-cadherin for immunocytochemical analysis. From our experiments, we found that TRPM7 co-localized with endogenous E-cadherin to the same depth in the cells, which indicates that TRPM7 localizes to adherens junctions in epithelial cells (Figure 20).

As a first step toward understanding TRPM7 role in cell-cell adhesion, we evaluated whether TRPM7 channel modulators would alter the cell adhesion pattern of E-cadherin, a marker of adherens junctions, in OK cells. We expected to observe that the inhibitor would reduce the level of junction formation, and that a TRPM7 channel opener would in contrast, enhance the adherens junction formation. The analysis of confocal images showed that treating cells with the TRPM7 channel inhibitor diminished the adherens junction accumulation as we expected. Treatment of cells with the TRPM7

channel opener, Naltriben mesylate, increased the expression of E-cadherin, however, the activation of TRPM7 seemed also to disrupt the localization of E-cadherin in the adherens junctions (Figure 21) [102, 103]. Thus, TRPM7 may be affecting both E-cadherin expression and localization; further investigations are necessary to elucidate the channels impact on cell-cell adhesion. For example, TRPM7 channel also conducts Ca^{2+} and the cadherin interactions in cell-cell junctions are known to be sensitive to calcium. In future investigations we would like to examine whether the effect of TRPM7 on E-cadherin localization is calcium-dependent [104]. We have published the results that TRPM7 channel localization is dependent upon its kinase activity [25]. Moreover, there have been several serine and threonine phosphorylation sites found in E-cadherin, which have important roles in its cell surface stability and adhesion activity [105, 106]. Therefore, it is worth investigating whether the kinase activity of TRPM7 influences E-cadherin activity or localization.

Another aim of my thesis project is to determine the mechanism by which TRPM7's function in proximal tubule is regulated. I proposed a working model in the rationale section of my thesis (Figure 4). A PDZ-scaffold protein family called NHERF was identified as the potential regulators of TRPM7 in kidney, using a yeast-two-hybrid screen of a mouse kidney library with the COOH-terminus of TRPM7 used as a bait. The NHERF family, especially NHERF1 and NHERF3, which have exclusive expression in the proximal tubule of kidney, have been reported to regulate a number of ion channels and transporters in proximal tubular cells. NHERFs usually regulate its binding partners through a small segment of amino acid called PDZ-binding motif. By interacting with ion channels or transporters via their PDZ-binding motifs, NHERFs tethered these membrane proteins to the plasma membrane, where they can perform their function of transporting

ions and small molecules into or out of cells. TRPM7 was found to have a class II motif that is extremely conserved across species. Deletion of this PDZ-binding motif from the COOH-terminus of TRPM7 did not affect its expression level and current intensity in HEK293 cells. However, the deletion the channel's PDZ-binding motif did shorten the retention time of the mutant TRPM7 (TRPM7ΔPDZ) to adherens junctions in OK cells, compared to TRPM7 WT, indicating that TRPM7 localization in the proximal tubule cells is regulated by the channel's PDZ-binding motif (Figure 23).

Using immunocytochemical analysis, we have detected that TRPM7 is more readily localized to the basolateral membrane in the OK cells and to a lesser extent at the apical membrane. We speculate that the limited localization of TRPM7 to the apical membrane was due to a shortage of scaffolding proteins to properly traffic or tether the overexpressed TRPM7 to the apical membrane, where we expect the channel to be also localized. Since we have confirmed the functional significance of PDZ-binding motif in TRPM7's localization, we next investigated whether the scaffolding NHERF proteins are the proteins that bring TRPM7 to the apical membrane by binding to the channel's PDZ-binding motif. We examined the localization of TRPM7 in response to co-expression of each of the 4 members of NHERF family. After 48 h of expression, cells were fixed and subjected to immunocytochemical analysis. TRPM7 was found readily localized to the basolateral side of OK cells, but in some cells, it showed weak localization to the apical side of the cell. In contrast, NHERF proteins were prominently found in cytosol and on the apical membrane. We did observe weak co-localization of TRPM7 with NHERF1 or NHERF3 in some cells, however, it was not enough to draw the conclusion that NHERF1 or NHERF3 regulates TRPM7 channel localization *in vivo* (Figure 24A). We also investigated whether NHERF proteins' presence would affect the localization pattern of

TRPM7. Statistical analysis of the ability of TRPM7 to localize to the cell periphery suggested that co-transfection of NHERF proteins with TRPM7 did not alter the channel's ability to localize to the cell periphery, which indicates that TRPM7 is not regulated by NHERF proteins (Figure 24B). This result was surprising at first because we initially hypothesized that TRPM7's function in proximal tubules was to reabsorb Mg^{2+}, which would require TRPM7 to localize to the apical membrane to function. However, our data showed that TRPM7 readily localized to the cell adherens junctions on lateral membranes instead of apical membranes, and that the channel's major function is not to reabsorb Mg^{2+} but to regulate the cell-cell adhesion process. We, however, cannot rule out that TRPM7 functions at both sites in proximal tubule cells. More study is required to test this conjecture.

As we proposed in the working model, we hypothesized that the channel's localization to apical membranes is controlled by NHERF proteins connected to PLC-mediated G-protein coupled receptor pathways. Even though NHERF proteins has been found not to be the responsible factors to traffic TRPM7 to the cell membrane and the TRPM7 was not responsible for Mg^{2+} reabsorption, we were still able to detect that TRPM7's localization in OK cells is influenced by PKC, as suggested by experiments using PKC inhibitors and activators (Figure 25). Our data indicates that TRPM7 localization is potentially regulated through the PKC pathway, which would be consistent with studies showing that activation of G protein coupled receptors potentiates TRPM7 channel activity [9].

In conclusion, our data in this study suggested that TRPM7's role in proximal tubule is to regulate the cell-cell adhesion process in adherens junctions rather than maintain the whole-body Mg^{2+} homeostasis (Figure 26). The evidence we obtained thus

far in support of this conclusion are summarized as following: 1. Tissue-specific knockout of TRPM7 in mouse renal proximal tubule did not cause Mg^{2+}-deficiency in mouse. 2. gGT-Cre *KO trpm7* mice exhibited more impaired intercellular junctions than *Trpm7*$^{flox/flox}$ control littermates in cortex of kidney. 3. TRPM7 was found to readily localize to the basolateral side instead of the apical side of the model cells (OK cells). 4. TRPM7 was found to co-localize with adherens junction proteins, plakoglobin and E-cadherin. 5. Blocking TRPM7's channel function reduced adherens junction formation in OK cells.

Our understanding of the relationship between TRPM7 and cell-cell adhesion is still in its infancy. We anticipated that the discoveries made in this study will guide future investigations of the role of the channel regulating cell-cell adhesion. Questions that remain unanswered that are ripe for future investigation include: What is the role of TRPM7 in regulating the formation of adherens junctions? Is the channel involved in directly regulating cell-cell adhesion? What is the role of TRPM7's channel and kinase domains in cell-cell adhesion? Is TRPM7 required to hold the junctions together to resist mechanical stress? To address these questions, we will perform knockdown assays on TRPM7 in model cells (e.g., OK cells or other established epithelial cell models) and analyze how the loss of function of TRPM7 affects the cell-cell adhesion itself as well as the assembly and disassembly of adherens junctions. Future work will also concentrate on understanding the origin of the renal cavities generated in gGT-Cre *KO trpm7* mice, which seems not to be due to a developmental problem, since the cavities appeared after the maturation of the *Trpm7 KO* mice.

In this study, we also investigated mechanism(s) by which TRPM7's function is regulated. We identified a regulatory site at the COOH-term of TRPM7, the channel's PDZ-binding motif, through which the localization of TRPM7 to cell periphery could be

regulated. Our investigations revealed that the PDZ scaffolding protein candidates we proposed to traffic TRPM7 to the apical membrane, NHERF proteins, were not involved in modulating TRPM7's cellular localization. Nevertheless, the proposed candidate PLC-mediated cell signaling pathway, PKC pathway was found to be involved in modulating TRPM7's localization in cells. Treatment of cells with the PKC inhibitor and activator produced opposite effects on TRPM's localization to the cell periphery. Based on the original working model and the data we obtained in this study, future studies should be devoted to identifying the PDZ scaffolding proteins that interact with TRPM7's PDZ-binding motif to regulate the channel's localization to cell periphery. We speculate that the PDZ-containing protein will either be localized to adherens junctions or regulate trafficking of proteins to this cellular site (Figure 26). In addition, we will continue to explore the mechanisms by which TRPM7 is regulated, such identifying which G-protein coupled receptors are involved in the regulation of the channel, and whether TRPM7's function is under the control of hormonal stimulation.

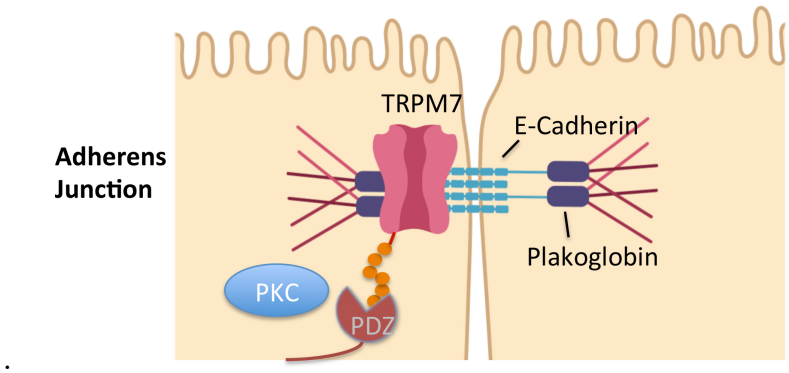

Figure 26. Proposed model of the TRPM7's function in cell-cell adhesion

In proximal tubule epithelial cells, TRPM7 channel localizes to adherens junctions to regulate the cell-cell adhesion between cells. It interacts with plakoglobin and regulates E-cadherin protein expression level and cellular localization. The TRPM7's localization to adherens junctions and its function in cell-cell adhesion are regulated through its PDZ-binding motif, and potentially mediated by the PKC pathway.

APPENDICES

Appendix 1. Primers for cloning

FLAG-NHERF2	Forward: CAT CAT AAG CTT ATG GCG GCG CCG GAG CCG CT Reverse: CAT CAT GAA TTC TCA GAA GTT GCT GAA GAT TTC ACG CTT CCT GTT CCA.
FLAG-NHERF4	Forward: CAT CAT AAG CTT ATG GAG AAA GCC GCA GAT CTG CAG GAC Reverse: CAT CAT GAA TTC CTA CAG TAG ATC CGA GGC CAG AGC C GAT CTG CAG GAC
HA-TRPM7ΔPDZ Quickchange	Top: GAA TCA GAA GCA ACA AAT TGA GTT CGT CTG ATG TTA TAG Bottom: CTA TAA CAT CAG ACG AAC TCA ATT TGT TGC TTC TGA TTC
C47ΔPDZ Quickchange	Top: GAA TCA GAA GCA ACA AAT TGA GTT CGT CTG ATG TTA TAG G Bottom: CCT ATA ACA TCA GAC GAA CTC AAT TTG TTG CTT CTG ATT

Appendix 2. Primers and PCR conditions for mouse genotyping

The primer sets and PCR conditions are as following:

For *Trpm7* flox allele, the primer sequence was:

5'-TAG CCC TGT AGA GTT TTA CTG G-3' and

5'-GAT AGA CTA TAT ACT AGG TAC ATG G-3'.

The 25 μL PCR reactions were set up as following:

Premix Buffer E (Promega, #M07205E)	12.5 μL
Forward primer	1 μL
Reverse primer	1 μL
Taq polymerase (Genscript, NJ)	0.5 μL
H_2O	18 μL
DNA template	2 μL

PCR conditions is as following:

Initial denaturing	95 °C for 10 min
Then 26 cycles of	95 °C for 30 sec
	60 °C for 30 sec

	72 °C for 90 sec
Extension	72 °C for 10 min

For gGT-Cre allele, the primer sequence was:

5'-GCT CTT GGG AGA AGT CAT GC-3' and

5'-CAT GTT TAG CTG GCC CAA AT-3'

The 25 μL PCR reactions were set up as following:

Taq Buffer	2.5 μL
Forward primer	0.5 μL
Reverse primer	0.5 μL
*d*NTP	0.5 μL
Taq polymerase	0.5 μL
H_2O	18.5 μL
DNA template	2 μL

PCR conditions is as following:

Initial denaturing	94 °C for 3 min

Then 26 cycles of	94 °C for 30 sec 56 °C for 45 sec 72 °C for 60 sec
Extension	72 °C for 7 min

For PEPCK-Cre allele, the primer sequence was:

5'-GCG GTC TGG GAG TAA AAA CTA TC-3' and

5'-GTG AAA CAG GAT TGC TGT GAG TT-3'

The 25 μL PCR reactions were set up as following:

Premix Buffer C (Promega, #FSP995C)	12.5 μL
Forward primer	1 μL
Reverse primer	1 μL
Taq polymerase	0.5 μL
H_2O	18 μL
DNA template	2 μL

PCR conditions is as following:

Initial denaturing	95 °C for 10 min
Then 26 cycles of	95 °C for 30 sec 60 °C for 30 sec 72 °C for 90 sec
Extension	72 °C for 10 min

ABBREVIATIONS

a.a., amino acid

ATCC, American Type Culture Collection

ATP, adenosine 5-triphosphate

Bis-Tris, Bis-(2-hydroxy-ethyl)-amino-tris(hydroxymethyl)-methane

BSA, bovine serum albumin

CC, coiled-coil

CCC, cadherin-catenin complex

DAPI, 4',6-diamidino-2-phenylindole

DCT, distal convoluted tubule

Disc-large, *Drosophila* junctional protein

D-MEM, Dulbecco's Modified Eagle Medium

DMSO, dimethyl sulfoxide

Dsg, desmoglein

Dsc, desmocollins

eEF2K, eukaryotic elongation factor-2 kinase

FBS, fetal bovine serum

GFP, green fluorescent protein

GPCR, G protein-coupled receptors

gGT γ-glutamyl transferase

GST, glutathione S-transferase

HA, hemagglutinin

HEK, human embryonic kidney

IP, immunoprecipitation

IPTG, isopropyl-β-D-1-thiogalactopyranoside

KO, knockout

LOH, loop of Henle

MHCK, myosin heavy chain kinase

MIC, magnesium-inhibited cation

MS, mass spectrometry

NHERF, sodium-hydrogen antiporter 3 regulator

Npt2a, sodium-dependent phosphate transporter

OK, opossum kidney

PBS, phosphate buffered saline

PBST, phosphate buffered saline-1% Triton-X100

PCR, polymerase chain reaction

PCT, proximal convoluted tubule

PDZ, acronym of the postsynaptic density protein PSD-95, the *Drosophila* junctional protein Disc-large, and the tight junction protein ZO1

PEPCK phosphoenolpyruvate carboxylkinase

PKA, protein kinase A

PKC, protein kinase C

PLC, phospholipase C

PMA Phorbol 12-myristate 13-acetate

PSD-95, postsynaptic density protein

PVDF, polyvinylidene difluoride

SDS, sodium dodecyl sulfate

SDS-PAGE, sodium dodecyl sulfate-polyacrylamide gel electrophoresis

S/T, serine/threonine-rich

TAL, thick ascending limb

TET, tetracycline

TEM, transmission electron microscopy

TRP, transient receptor potential

TRPM, transient receptor potential melastatin

WT, wild-type

REFERENCES

1. Nilius, B., G. Owsianik, T. Voets, and J.A. Peters, *Transient receptor potential cation channels in disease.* Physiol Rev, 2007. **87**(1): p. 165-217.
2. Runnels, L.W., *TRPM6 and TRPM7: A Mul-TRP-PLIK-cation of channel functions.* Curr Pharm Biotechnol, 2011. **12**(1): p. 42-53.
3. Runnels, L.W., L. Yue, and D.E. Clapham, *TRP-PLIK, a bifunctional protein with kinase and ion channel activities.* Science, 2001. **291**(5506): p. 1043-7.
4. Nadler, M.J., M.C. Hermosura, K. Inabe, A.L. Perraud, Q. Zhu, A.J. Stokes, T. Kurosaki, J.P. Kinet, R. Penner, A.M. Scharenberg, and A. Fleig, *LTRPC7 is a Mg.ATP-regulated divalent cation channel required for cell viability.* Nature, 2001. **411**(6837): p. 590-5.
5. Paravicini, T.M., V. Chubanov, and T. Gudermann, *TRPM7: a unique channel involved in magnesium homeostasis.* Int J Biochem Cell Biol, 2012. **44**(8): p. 1381-4.
6. Monteilh-Zoller, M.K., M.C. Hermosura, M.J. Nadler, A.M. Scharenberg, R. Penner, and A. Fleig, *TRPM7 provides an ion channel mechanism for cellular entry of trace metal ions.* J Gen Physiol, 2003. **121**(1): p. 49-60.
7. Demeuse, P., R. Penner, and A. Fleig, *TRPM7 channel is regulated by magnesium nucleotides via its kinase domain.* J Gen Physiol, 2006. **127**(4): p. 421-34.
8. Kozak, J.A., M. Matsushita, A.C. Nairn, and M.D. Cahalan, *Charge screening by internal pH and polyvalent cations as a mechanism for activation, inhibition, and rundown of TRPM7/MIC channels.* J Gen Physiol, 2005. **126**(5): p. 499-514.
9. Runnels, L.W., L. Yue, and D.E. Clapham, *The TRPM7 channel is inactivated by PIP(2) hydrolysis.* Nat Cell Biol, 2002. **4**(5): p. 329-36.
10. Yu, H., Z. Zhang, A. Lis, R. Penner, and A. Fleig, *TRPM7 is regulated by halides through its kinase domain.* Cell Mol Life Sci, 2013. **70**(15): p. 2757-71.
11. Luck-Vielmetter, D., M. Schleicher, B. Grabatin, J. Wippler, and G. Gerisch, *Replacement of threonine residues by serine and alanine in a phosphorylatable heavy chain fragment of Dictyostelium myosin II.* FEBS Lett, 1990. **269**(1): p. 239-43.
12. Vaillancourt, J.P., C. Lyons, and G.P. Cote, *Identification of two phosphorylated threonines in the tail region of Dictyostelium myosin II.* J Biol Chem, 1988. **263**(21): p. 10082-7.
13. Dorovkov, M.V. and A.G. Ryazanov, *Phosphorylation of annexin I by TRPM7 channel-kinase.* J Biol Chem, 2004. **279**(49): p. 50643-6.
14. Clark, K., M. Langeslag, B. van Leeuwen, L. Ran, A.G. Ryazanov, C.G. Figdor, W.H. Moolenaar, K. Jalink, and F.N. van Leeuwen, *TRPM7, a novel regulator of actomyosin contractility and cell adhesion.* Embo j, 2006. **25**(2): p. 290-301.
15. Clark, K., J. Middelbeek, E. Lasonder, N.G. Dulyaninova, N.A. Morrice, A.G. Ryazanov, A.R. Bresnick, C.G. Figdor, and F.N. van Leeuwen, *TRPM7 regulates myosin IIA filament stability and protein localization by heavy chain phosphorylation.* J Mol Biol, 2008. **378**(4): p. 790-803.
16. Deason-Towne, F., A.L. Perraud, and C. Schmitz, *Identification of Ser/Thr phosphorylation sites in the C2-domain of phospholipase C gamma2 (PLCgamma2) using TRPM7-kinase.* Cell Signal, 2012. **24**(11): p. 2070-5.

17. Perraud, A.L., X. Zhao, A.G. Ryazanov, and C. Schmitz, *The channel-kinase TRPM7 regulates phosphorylation of the translational factor eEF2 via eEF2-k.* Cell Signal, 2011. **23**(3): p. 586-93.
18. Yamaguchi, H., M. Matsushita, A.C. Nairn, and J. Kuriyan, *Crystal structure of the atypical protein kinase domain of a TRP channel with phosphotransferase activity.* Mol Cell, 2001. **7**(5): p. 1047-57.
19. Ryazanova, L.V., M.V. Dorovkov, A. Ansari, and A.G. Ryazanov, *Characterization of the protein kinase activity of TRPM7/ChaK1, a protein kinase fused to the transient receptor potential ion channel.* J Biol Chem, 2004. **279**(5): p. 3708-16.
20. Clark, K., J. Middelbeek, N.A. Morrice, C.G. Figdor, E. Lasonder, and F.N. van Leeuwen, *Massive autophosphorylation of the Ser/Thr-rich domain controls protein kinase activity of TRPM6 and TRPM7.* PLoS One, 2008. **3**(3): p. e1876.
21. Cai, N., Z. Bai, V. Nanda, and L.W. Runnels, *Mass Spectrometric Analysis of TRPM6 and TRPM7 Phosphorylation Reveals Regulatory Mechanisms of the Channel-Kinases.* Sci Rep, 2017. **7**: p. 42739.
22. Schmitz, C., A.L. Perraud, C.O. Johnson, K. Inabe, M.K. Smith, R. Penner, T. Kurosaki, A. Fleig, and A.M. Scharenberg, *Regulation of vertebrate cellular Mg2+ homeostasis by TRPM7.* Cell, 2003. **114**(2): p. 191-200.
23. Matsushita, M., J.A. Kozak, Y. Shimizu, D.T. McLachlin, H. Yamaguchi, F.Y. Wei, K. Tomizawa, H. Matsui, B.T. Chait, M.D. Cahalan, and A.C. Nairn, *Channel function is dissociated from the intrinsic kinase activity and autophosphorylation of TRPM7/ChaK1.* J Biol Chem, 2005. **280**(21): p. 20793-803.
24. Su, L.T., M.A. Agapito, M. Li, W.T. Simonson, A. Huttenlocher, R. Habas, L. Yue, and L.W. Runnels, *TRPM7 regulates cell adhesion by controlling the calcium-dependent protease calpain.* J Biol Chem, 2006. **281**(16): p. 11260-70.
25. Cai, N., L. Lou, N. Al-Saadi, S. Tetteh, and L.W. Runnels, *The kinase activity of the channel-kinase protein TRPM7 regulates stability and localization of the TRPM7 channel in polarized epithelial cells.* J Biol Chem, 2018. **293**(29): p. 11491-11504.
26. Ryazanova, L.V., L.J. Rondon, S. Zierler, Z. Hu, J. Galli, T.P. Yamaguchi, A. Mazur, A. Fleig, and A.G. Ryazanov, *TRPM7 is essential for Mg(2+) homeostasis in mammals.* Nat Commun, 2010. **1**: p. 109.
27. Schappe, M.S., K. Szteyn, M.E. Stremska, S.K. Mendu, T.K. Downs, P.V. Seegren, M.A. Mahoney, S. Dixit, J.K. Krupa, E.J. Stipes, J.S. Rogers, S.E. Adamson, N. Leitinger, and B.N. Desai, *Chanzyme TRPM7 Mediates the Ca(2+) Influx Essential for Lipopolysaccharide-Induced Toll-Like Receptor 4 Endocytosis and Macrophage Activation.* Immunity, 2018. **48**(1): p. 59-74.e5.
28. Abiria, S.A., G. Krapivinsky, R. Sah, A.G. Santa-Cruz, D. Chaudhuri, J. Zhang, P. Adstamongkonkul, P.G. DeCaen, and D.E. Clapham, *TRPM7 senses oxidative stress to release Zn(2+) from unique intracellular vesicles.* Proc Natl Acad Sci U S A, 2017. **114**(30): p. E6079-e6088.
29. Desai, B.N., G. Krapivinsky, B. Navarro, L. Krapivinsky, B.C. Carter, S. Febvay, M. Delling, A. Penumaka, I.S. Ramsey, Y. Manasian, and D.E. Clapham, *Cleavage of TRPM7 releases the kinase domain from the ion channel and regulates its participation in Fas-induced apoptosis.* Dev Cell, 2012. **22**(6): p. 1149-62.

30. Chen, K.H., X.H. Xu, Y. Liu, Y. Hu, M.W. Jin, and G.R. Li, *TRPM7 channels regulate proliferation and adipogenesis in 3T3-L1 preadipocytes.* J Cell Physiol, 2014. **229**(1): p. 60-7.
31. Zierler, S., G. Yao, Z. Zhang, W.C. Kuo, P. Porzgen, R. Penner, F.D. Horgen, and A. Fleig, *Waixenicin A inhibits cell proliferation through magnesium-dependent block of transient receptor potential melastatin 7 (TRPM7) channels.* J Biol Chem, 2011. **286**(45): p. 39328-35.
32. Sahni, J. and A.M. Scharenberg, *TRPM7 ion channels are required for sustained phosphoinositide 3-kinase signaling in lymphocytes.* Cell Metab, 2008. **8**(1): p. 84-93.
33. Wei, C., X. Wang, M. Chen, K. Ouyang, L.S. Song, and H. Cheng, *Calcium flickers steer cell migration.* Nature, 2009. **457**(7231): p. 901-5.
34. Meng, X., C. Cai, J. Wu, S. Cai, C. Ye, H. Chen, Z. Yang, H. Zeng, Q. Shen, and F. Zou, *TRPM7 mediates breast cancer cell migration and invasion through the MAPK pathway.* Cancer Lett, 2013. **333**(1): p. 96-102.
35. Kuras, Z., Y.H. Yun, A.A. Chimote, L. Neumeier, and L. Conforti, *KCa3.1 and TRPM7 channels at the uropod regulate migration of activated human T cells.* PLoS One, 2012. **7**(8): p. e43859.
36. Su, L.T., W. Liu, H.C. Chen, O. Gonzalez-Pagan, R. Habas, and L.W. Runnels, *TRPM7 regulates polarized cell movements.* Biochem J, 2011. **434**(3): p. 513-21.
37. Zhang, Z., M. Wang, X.H. Fan, J.H. Chen, Y.Y. Guan, and Y.B. Tang, *Upregulation of TRPM7 channels by angiotensin II triggers phenotypic switching of vascular smooth muscle cells of ascending aorta.* Circ Res, 2012. **111**(9): p. 1137-46.
38. Abed, E., C. Martineau, and R. Moreau, *Role of melastatin transient receptor potential 7 channels in the osteoblastic differentiation of murine MC3T3 cells.* Calcif Tissue Int, 2011. **88**(3): p. 246-53.
39. Zhang, Y., J. Xu, Y.C. Ruan, M.K. Yu, M. O'Laughlin, H. Wise, D. Chen, L. Tian, D. Shi, J. Wang, S. Chen, J.Q. Feng, D.H. Chow, X. Xie, L. Zheng, L. Huang, S. Huang, K. Leung, N. Lu, L. Zhao, H. Li, D. Zhao, X. Guo, K. Chan, F. Witte, H.C. Chan, Y. Zheng, and L. Qin, *Implant-derived magnesium induces local neuronal production of CGRP to improve bone-fracture healing in rats.* Nat Med, 2016. **22**(10): p. 1160-1169.
40. Nadolni, W. and S. Zierler, *The Channel-Kinase TRPM7 as Novel Regulator of Immune System Homeostasis.* Cells, 2018. **7**(8).
41. Brauchi, S., G. Krapivinsky, L. Krapivinsky, and D.E. Clapham, *TRPM7 facilitates cholinergic vesicle fusion with the plasma membrane.* Proc Natl Acad Sci U S A, 2008. **105**(24): p. 8304-8.
42. Numata, T., T. Shimizu, and Y. Okada, *Direct mechano-stress sensitivity of TRPM7 channel.* Cell Physiol Biochem, 2007. **19**(1-4): p. 1-8.
43. Du, J., J. Xie, Z. Zhang, H. Tsujikawa, D. Fusco, D. Silverman, B. Liang, and L. Yue, *TRPM7-mediated Ca2+ signals confer fibrogenesis in human atrial fibrillation.* Circ Res, 2010. **106**(5): p. 992-1003.
44. Touyz, R.M., *Transient receptor potential melastatin 6 and 7 channels, magnesium transport, and vascular biology: implications in hypertension.* Am J Physiol Heart Circ Physiol, 2008. **294**(3): p. H1103-18.
45. Antunes, T.T., G.E. Callera, Y. He, A. Yogi, A.G. Ryazanov, L.V. Ryazanova, A. Zhai, D.J. Stewart, A. Shrier, and R.M. Touyz, *Transient Receptor Potential*

Melastatin 7 Cation Channel Kinase: New Player in Angiotensin II-Induced Hypertension. Hypertension, 2016. **67**(4): p. 763-73.

46. Aarts, M., K. Iihara, W.L. Wei, Z.G. Xiong, M. Arundine, W. Cerwinski, J.F. MacDonald, and M. Tymianski, *A key role for TRPM7 channels in anoxic neuronal death.* Cell, 2003. **115**(7): p. 863-77.
47. Guilbert, A., M. Gautier, I. Dhennin-Duthille, N. Haren, H. Sevestre, and H. Ouadid-Ahidouch, *Evidence that TRPM7 is required for breast cancer cell proliferation.* Am J Physiol Cell Physiol, 2009. **297**(3): p. C493-502.
48. Kim, B.J., E.J. Park, J.H. Lee, J.H. Jeon, S.J. Kim, and I. So, *Suppression of transient receptor potential melastatin 7 channel induces cell death in gastric cancer.* Cancer Sci, 2008. **99**(12): p. 2502-9.
49. Jin, J., B.N. Desai, B. Navarro, A. Donovan, N.C. Andrews, and D.E. Clapham, *Deletion of Trpm7 disrupts embryonic development and thymopoiesis without altering Mg2+ homeostasis.* Science, 2008. **322**(5902): p. 756-60.
50. Jin, J., L.J. Wu, J. Jun, X. Cheng, H. Xu, N.C. Andrews, and D.E. Clapham, *The channel kinase, TRPM7, is required for early embryonic development.* Proc Natl Acad Sci U S A, 2012. **109**(5): p. E225-33.
51. Elizondo, M.R., B.L. Arduini, J. Paulsen, E.L. MacDonald, J.L. Sabel, P.D. Henion, R.A. Cornell, and D.M. Parichy, *Defective skeletogenesis with kidney stone formation in dwarf zebrafish mutant for trpm7.* Curr Biol, 2005. **15**(7): p. 667-71.
52. Liu, W., L.T. Su, D.K. Khadka, C. Mezzacappa, Y. Komiya, A. Sato, R. Habas, and L.W. Runnels, *TRPM7 regulates gastrulation during vertebrate embryogenesis.* Dev Biol, 2011. **350**(2): p. 348-57.
53. Watanabe, M., Y. Suzuki, K. Uchida, N. Miyazaki, K. Murata, S. Matsumoto, H. Kakizaki, and M. Tominaga, *Trpm7 Protein Contributes to Intercellular Junction Formation in Mouse Urothelium.* J Biol Chem, 2015. **290**(50): p. 29882-92.
54. Chubanov, V., S. Waldegger, M. Mederos y Schnitzler, H. Vitzthum, M.C. Sassen, H.W. Seyberth, M. Konrad, and T. Gudermann, *Disruption of TRPM6/TRPM7 complex formation by a mutation in the TRPM6 gene causes hypomagnesemia with secondary hypocalcemia.* Proc Natl Acad Sci U S A, 2004. **101**(9): p. 2894-9.
55. Ryazanova, L.V., Z. Hu, S. Suzuki, V. Chubanov, A. Fleig, and A.G. Ryazanov, *Elucidating the role of the TRPM7 alpha-kinase: TRPM7 kinase inactivation leads to magnesium deprivation resistance phenotype in mice.* Sci Rep, 2014. **4**: p. 7599.
56. Chubanov, V., S. Ferioli, A. Wisnowsky, D.G. Simmons, C. Leitzinger, C. Einer, W. Jonas, Y. Shymkiv, H. Bartsch, A. Braun, B. Akdogan, L. Mittermeier, L. Sytik, F. Torben, V. Jurinovic, E.P. van der Vorst, C. Weber, O.A. Yildirim, K. Sotlar, A. Schurmann, S. Zierler, H. Zischka, A.G. Ryazanov, and T. Gudermann, *Epithelial magnesium transport by TRPM6 is essential for prenatal development and adult survival.* Elife, 2016. **5**.
57. Schmitz, C., M.V. Dorovkov, X. Zhao, B.J. Davenport, A.G. Ryazanov, and A.L. Perraud, *The channel kinases TRPM6 and TRPM7 are functionally nonredundant.* J Biol Chem, 2005. **280**(45): p. 37763-71.
58. Schlingmann, K.P., S. Weber, M. Peters, L. Niemann Nejsum, H. Vitzthum, K. Klingel, M. Kratz, E. Haddad, E. Ristoff, D. Dinour, M. Syrrou, S. Nielsen, M. Sassen, S. Waldegger, H.W. Seyberth, and M. Konrad, *Hypomagnesemia with*

secondary hypocalcemia is caused by mutations in TRPM6, a new member of the TRPM gene family. Nat Genet, 2002. **31**(2): p. 166-70.
59. Walder, R.Y., D. Landau, P. Meyer, H. Shalev, M. Tsolia, Z. Borochowitz, M.B. Boettger, G.E. Beck, R.K. Englehardt, R. Carmi, and V.C. Sheffield, *Mutation of TRPM6 causes familial hypomagnesemia with secondary hypocalcemia.* Nat Genet, 2002. **31**(2): p. 171-4.
60. Mittermeier, L., L. Demirkhanyan, B. Stadlbauer, A. Breit, C. Recordati, A. Hilgendorff, M. Matsushita, A. Braun, D.G. Simmons, E. Zakharian, T. Gudermann, and V. Chubanov, *TRPM7 is the central gatekeeper of intestinal mineral absorption essential for postnatal survival.* Proc Natl Acad Sci U S A, 2019.
61. Weinman, E.J., D. Steplock, Y. Wang, and S. Shenolikar, *Characterization of a protein cofactor that mediates protein kinase A regulation of the renal brush border membrane Na(+)-H+ exchanger.* J Clin Invest, 1995. **95**(5): p. 2143-9.
62. Kim, E., M. Niethammer, A. Rothschild, Y.N. Jan, and M. Sheng, *Clustering of Shaker-type K+ channels by interaction with a family of membrane-associated guanylate kinases.* Nature, 1995. **378**(6552): p. 85-8.
63. Tsunoda, S. and C.S. Zuker, *The organization of INAD-signaling complexes by a multivalent PDZ domain protein in Drosophila photoreceptor cells ensures sensitivity and speed of signaling.* Cell Calcium, 1999. **26**(5): p. 165-71.
64. Sheng, M. and C. Sala, *PDZ domains and the organization of supramolecular complexes.* Annu Rev Neurosci, 2001. **24**: p. 1-29.
65. Thelin, W.R., C.A. Hodson, and S.L. Milgram, *Beyond the brush border: NHERF4 blazes new NHERF turf.* J Physiol, 2005. **567**(Pt 1): p. 13-9.
66. Ardura, J.A. and P.A. Friedman, *Regulation of G protein-coupled receptor function by Na+/H+ exchange regulatory factors.* Pharmacol Rev, 2011. **63**(4): p. 882-900.
67. Shenolikar, S., J.W. Voltz, R. Cunningham, and E.J. Weinman, *Regulation of ion transport by the NHERF family of PDZ proteins.* Physiology (Bethesda), 2004. **19**: p. 362-9.
68. Mahon, M.J., J.A. Cole, E.D. Lederer, and G.V. Segre, *Na+/H+ exchanger-regulatory factor 1 mediates inhibition of phosphate transport by parathyroid hormone and second messengers by acting at multiple sites in opossum kidney cells.* Mol Endocrinol, 2003. **17**(11): p. 2355-64.
69. de Baaij, J.H., J.G. Hoenderop, and R.J. Bindels, *Magnesium in man: implications for health and disease.* Physiol Rev, 2015. **95**(1): p. 1-46.
70. Escuela, M.P., M. Guerra, J.M. Anon, V. Martinez-Vizcaino, M.D. Zapatero, A. Garcia-Jalon, and S. Celaya, *Total and ionized serum magnesium in critically ill patients.* Intensive Care Med, 2005. **31**(1): p. 151-6.
71. Khan, A.M., S.A. Lubitz, L.M. Sullivan, J.X. Sun, D. Levy, R.S. Vasan, J.W. Magnani, P.T. Ellinor, E.J. Benjamin, and T.J. Wang, *Low serum magnesium and the development of atrial fibrillation in the community: the Framingham Heart Study.* Circulation, 2013. **127**(1): p. 33-8.
72. Lutsey, P.L., A. Alonso, E.D. Michos, L.R. Loehr, B.C. Astor, J. Coresh, and A.R. Folsom, *Serum magnesium, phosphorus, and calcium are associated with risk of incident heart failure: the Atherosclerosis Risk in Communities (ARIC) Study.* Am J Clin Nutr, 2014. **100**(3): p. 756-64.

73. Qu, X., F. Jin, Y. Hao, H. Li, T. Tang, H. Wang, W. Yan, and K. Dai, *Magnesium and the risk of cardiovascular events: a meta-analysis of prospective cohort studies.* PLoS One, 2013. **8**(3): p. e57720.
74. Dalton, L.M., D.M. Ni Fhloinn, G.T. Gaydadzhieva, O.M. Mazurkiewicz, H. Leeson, and C.P. Wright, *Magnesium in pregnancy.* Nutr Rev, 2016. **74**(9): p. 549-57.
75. Takaya, J., F. Yamato, and K. Kaneko, *Possible relationship between low birth weight and magnesium status: from the standpoint of "fetal origin" hypothesis.* Magnes Res, 2006. **19**(1): p. 63-9.
76. Curry, J.N. and A.S.L. Yu, *Magnesium Handling in the Kidney.* Adv Chronic Kidney Dis, 2018. **25**(3): p. 236-243.
77. Shenolikar, S., J.W. Voltz, C.M. Minkoff, J.B. Wade, and E.J. Weinman, *Targeted disruption of the mouse NHERF-1 gene promotes internalization of proximal tubule sodium-phosphate cotransporter type IIa and renal phosphate wasting.* Proc Natl Acad Sci U S A, 2002. **99**(17): p. 11470-5.
78. Iwano, M., D. Plieth, T.M. Danoff, C. Xue, H. Okada, and E.G. Neilson, *Evidence that fibroblasts derive from epithelium during tissue fibrosis.* J Clin Invest, 2002. **110**(3): p. 341-50.
79. Overton, J.D., Y. Komiya, C. Mezzacappa, K. Nama, N. Cai, L. Lou, S.V. Fedeles, R. Habas, and L.W. Runnels, *Hepatocystin is Essential for TRPM7 Function During Early Embryogenesis.* Sci Rep, 2015. **5**: p. 18395.
80. Hanson, R.W. and L. Reshef, *Regulation of phosphoenolpyruvate carboxykinase (GTP) gene expression.* Annu Rev Biochem, 1997. **66**: p. 581-611.
81. Beale, E.G., D.E. Clouthier, and R.E. Hammer, *Cell-specific expression of cytosolic phosphoenolpyruvate carboxykinase in transgenic mice.* Faseb j, 1992. **6**(15): p. 3330-7.
82. Patel, Y.M., J.S. Yun, J. Liu, M.M. McGrane, and R.W. Hanson, *An analysis of regulatory elements in the phosphoenolpyruvate carboxykinase (GTP) gene which are responsible for its tissue-specific expression and metabolic control in transgenic mice.* J Biol Chem, 1994. **269**(8): p. 5619-28.
83. Schaffner, D.L., R. Barrios, C. Massey, E.I. Banez, C.N. Ou, S. Rajagopalan, E. Aguilar-Cordova, R.M. Lebovitz, P.A. Overbeek, and M.W. Lieberman, *Targeting of the rasT24 oncogene to the proximal convoluted tubules in transgenic mice results in hyperplasia and polycystic kidneys.* Am J Pathol, 1993. **142**(4): p. 1051-60.
84. Chobert, M.N., O. Lahuna, F. Lebargy, O. Kurauchi, M. Darbouy, J.F. Bernaudin, G. Guellaen, R. Barouki, and Y. Laperche, *Tissue-specific expression of two gamma-glutamyl transpeptidase mRNAs with alternative 5' ends encoded by a single copy gene in the rat.* J Biol Chem, 1990. **265**(4): p. 2352-7.
85. Quamme, G.A. and J.H. Dirks, *Magnesium transport in the nephron.* Am J Physiol, 1980. **239**(5): p. F393-401.
86. Matsuzaki, H., T. Nemoto, M. Fuchigami, M. Uehara, K. Suzuki, and K. Nakamura, *Effects of gender on kidney function in magnesium-deficient rats.* Biofactors, 2004. **22**(1-4): p. 43-6.
87. Quamme, G.A., *Renal magnesium handling: new insights in understanding old problems.* Kidney Int, 1997. **52**(5): p. 1180-95.

88. Lelievre-Pegorier, M., C. Merlet-Benichou, N. Roinel, and C. de Rouffignac, *Developmental pattern of water and electrolyte transport in rat superficial nephrons.* Am J Physiol, 1983. **245**(1): p. F15-21.
89. Zeng, Z., K. Inoue, H. Sun, T. Leng, X. Feng, L. Zhu, and Z.G. Xiong, *TRPM7 regulates vascular endothelial cell adhesion and tube formation.* Am J Physiol Cell Physiol, 2015. **308**(4): p. C308-18.
90. Weinman, E.J., D. Steplock, B. Cha, O. Kovbasnjuk, N.A. Frost, R. Cunningham, S. Shenolikar, T.A. Blanpied, and M. Donowitz, *PTH transiently increases the percent mobile fraction of Npt2a in OK cells as determined by FRAP.* Am J Physiol Renal Physiol, 2009. **297**(6): p. F1560-5.
91. Mahon, M.J. and G.V. Segre, *Stimulation by parathyroid hormone of a NHERF-1-assembled complex consisting of the parathyroid hormone I receptor, phospholipase Cbeta, and actin increases intracellular calcium in opossum kidney cells.* J Biol Chem, 2004. **279**(22): p. 23550-8.
92. Aberle, H., H. Schwartz, and R. Kemler, *Cadherin-catenin complex: protein interactions and their implications for cadherin function.* J Cell Biochem, 1996. **61**(4): p. 514-23.
93. Barth, A.I., I.S. Nathke, and W.J. Nelson, *Cadherins, catenins and APC protein: interplay between cytoskeletal complexes and signaling pathways.* Curr Opin Cell Biol, 1997. **9**(5): p. 683-90.
94. Franke, W.W., P.J. Koch, S. Schafer, H.W. Heid, S.M. Troyanovsky, I. Moll, and R. Moll, *The desmosome and the syndesmos: cell junctions in normal development and in malignancy.* Princess Takamatsu Symp, 1994. **24**: p. 14-27.
95. Steinberg, M.S., H. Shida, G.J. Giudice, M. Shida, N.H. Patel, and O.W. Blaschuk, *On the molecular organization, diversity and functions of desmosomal proteins.* Ciba Found Symp, 1987. **125**: p. 3-25.
96. Gumbiner, B.M., *Cell adhesion: the molecular basis of tissue architecture and morphogenesis.* Cell, 1996. **84**(3): p. 345-57.
97. Kim, J.K., O. Kwon, J. Kim, E.K. Kim, H.K. Park, J.E. Lee, K.L. Kim, J.W. Choi, S. Lim, H. Seok, W. Lee-Kwon, J.H. Choi, B.H. Kang, S. Kim, S.H. Ryu, and P.G. Suh, *PDZ domain-containing 1 (PDZK1) protein regulates phospholipase C-beta3 (PLC-beta3)-specific activation of somatostatin by forming a ternary complex with PLC-beta3 and somatostatin receptors.* J Biol Chem, 2012. **287**(25): p. 21012-24.
98. Hernando, N., S.M. Gisler, S. Pribanic, N. Deliot, P. Capuano, C.A. Wagner, O.W. Moe, J. Biber, and H. Murer, *NaPi-IIa and interacting partners.* J Physiol, 2005. **567**(Pt 1): p. 21-6.
99. Ozaki, M., H. Ogita, and Y. Takai, *Involvement of integrin-induced activation of protein kinase C in the formation of adherens junctions.* Genes Cells, 2007. **12**(5): p. 651-62.
100. Middelbeek, J., A.J. Kuipers, L. Henneman, D. Visser, I. Eidhof, R. van Horssen, B. Wieringa, S.V. Canisius, W. Zwart, L.F. Wessels, F.C. Sweep, P. Bult, P.N. Span, F.N. van Leeuwen, and K. Jalink, *TRPM7 is required for breast tumor cell metastasis.* Cancer Res, 2012. **72**(16): p. 4250-61.
101. Courjault, F., B. Gerin, D. Leroy, J. Chevalier, and H. Toutain, *Morphological and biochemical characterization of the opossum kidney cell line and primary cultures of rabbit proximal tubule cells in serum-free defined medium.* Cell Biol Int Rep, 1991. **15**(12): p. 1225-34.

102. Maslov, L.N., P.R. Oeltgen, Y.B. Lishmanov, S.A. Brown, E.I. Barzakh, A.V. Krylatov, and J.M. Pei, *Activation of peripheral delta opioid receptors increases cardiac tolerance to arrhythmogenic effect of ischemia/reperfusion.* Acad Emerg Med, 2014. **21**(1): p. 31-9.
103. Joly, N., A. El Aneed, P. Martin, R. Cecchelli, and J. Banoub, *Structural determination of the novel fragmentation routes of morphine opiate receptor antagonists using electrospray ionization quadrupole time-of-flight tandem mass spectrometry.* Rapid Commun Mass Spectrom, 2005. **19**(21): p. 3119-30.
104. Kim, S.A., C.Y. Tai, L.P. Mok, E.A. Mosser, and E.M. Schuman, *Calcium-dependent dynamics of cadherin interactions at cell-cell junctions.* Proc Natl Acad Sci U S A, 2011. **108**(24): p. 9857-62.
105. Chen, C.L., S.H. Wang, P.C. Chan, M.R. Shen, and H.C. Chen, *Phosphorylation of E-cadherin at threonine 790 by protein kinase Cdelta reduces beta-catenin binding and suppresses the function of E-cadherin.* Oncotarget, 2016. **7**(24): p. 37260-37276.
106. McEwen, A.E., M.T. Maher, R. Mo, and C.J. Gottardi, *E-cadherin phosphorylation occurs during its biosynthesis to promote its cell surface stability and adhesion.* Mol Biol Cell, 2014. **25**(16): p. 2365-74.